

Highlights

- Pt/C + ionomer catalyst layers prepared by electrospray deposition on Nafion membrane
- The layers show higher hydrogen mass transport rate compared with standard layers
- High mass transport rate in the layers also at very low Pt loading ($0.025 \text{ mg}\cdot\text{cm}^{-2}$)
- Enhanced water-vapor uptake capability and very low wettability (superhydrophobic)
- Electrosprayed layers combine high mass transport and high ionic conductivity

1
2
3
4
5
6
7
8
9
10
11
12
13
14
15
16
17
18
19
20
21
22
23
24
25
26
27
28
29
30
31
32
33
34
35
36
37
38
39
40
41
42
43
44
45
46
47
48
49
50
51
52
53
54
55
56
57
58
59
60
61
62
63
64
65

Mass-transport properties of electrosprayed Pt/C catalyst layers for polymer-electrolyte fuel cells.

Julio J. Conde¹, M. Antonia Folgado¹, P. Ferreira-Aparicio¹, Antonio M. Chaparro^{1,*},

Anamika Chowdhury², Ahmet Kusoglu², David Cullen³, Adam Z. Weber²

1) Energy Department, CIEMAT, Avda. Complutense 40. 28040 Madrid, Spain

2) Energy Conversion Group, Energy Technologies Area, Lawrence Berkeley National Laboratory, 1

Cyclotron Road, Berkeley, California 94720, USA

3) Center for Nanophase Materials Sciences, Oak Ridge National Laboratory, Oak Ridge, Tennessee

37831, USA

- Declarations of interest: none

*Corresponding author:

Antonio M. Chaparro

Energy Department, CIEMAT, Avda. Complutense 40. 28040 Madrid, Spain

antonio.mchaparro@ciemat.es

Telephone: +34 913460897

Fax: +34 913466269

1
2
3
4 ABSTRACT
5
6

7 Mass-transport properties of electro sprayed catalyst-layers based on Pt/C and ionomer (Nafion)
8 are studied with hydrogen limiting-current technique, water-vapor-uptake, scanning transmission
9 microscopy (STEM), single-cell testing, and impedance spectroscopy. The hydrogen limiting-
10 current technique provides the transport resistance of the layers (R_{cl}^{mt}), which shows to be lower
11 in electro sprayed layers compared with conventional layers, especially at very low platinum
12 loadings ($0.025 \text{ mg}_{\text{Pt}} \cdot \text{cm}^{-2}$) and low cell temperature, denoting superior mass-transport properties.
13
14 Images of the distribution of Pt, F, and C elements reveal the ionomer preferentially interacting
15 with the Pt nanoparticles. Water-vapor-uptake experiments show larger vapor absorption for
16 electro sprayed than conventional catalyst layers. Such large water-vapor uptake capability is
17 combined with superhydrophobicity, ie. very low interaction with water in liquid phase
18 (wettability). Both apparently contradictory properties result from a particular configuration of the
19 amphiphilic ionomer in the electro sprayed layers, and provide ideal conditions for high mass
20 transport and ionic conductivity in a catalyst layer. Electro sprayed layers as cathode catalyst layers
21 show peak response at a loading of $0.17 \text{ mg}_{\text{Pt}} \cdot \text{cm}^{-2}$ ($18 \mu\text{m}$ layer thickness when using Pt/C 20 wt%
22 catalyst) where they provide minimal mass-transport and polarization resistances.
23
24
25
26
27
28
29
30
31
32
33
34
35
36
37
38
39
40
41
42
43

44 Keywords: PEMFC, catalyst layer, electro spray, mass transport, water uptake, thin porous film
45
46
47
48
49
50
51
52
53
54
55
56
57
58
59
60
61
62
63
64
65

1. Introduction

Mass transport in the catalyst layer of proton-exchange-membrane fuel cells (PEMFCs) has a significant impact on fuel-cell performance and durability. Within the catalyst layer, mass transport of reactants (O_2 , H_2) and product (water) take place near the catalyst sites, resulting in local transport resistances that impact polarization behavior. In addition, the transport of liquid water in the catalyst layer controls the membrane and electrodes humidification states that determine key parameters for fuel cell performance, like the internal resistance and the catalyst activity. The catalyst layer must allow for facile transport of gas and liquid water, high proton conductivity, and easy accessibility of catalytic sites, keeping at the same time optimal membrane humidification [1,2,3].

A promising catalyst-layer fabrication technique is electrospray deposition, which enables one to produce catalyst layers with particular morphology, transport properties, and wettability [4,5,6,7,8,9]. The electrospray deposition uses a suspension of catalyst particles (Pt/C) and nanometer ionomer aggregates (Nafion) which is ejected through a nozzle under the influence of a strong electric field. By these means, the suspension is transferred to an aerosol of charged particles where the solvent evaporates, so they are dry deposited and discharged on the substrate under electrostatic interactions. The substrate can be the gas-diffusion layer (GDL) or the proton-exchange membrane [10]. Dendritic morphologies and a specific interaction between the catalyst and the ionomer have been observed in the electrosprayed films, however the exact nature is yet unknown. Under appropriate deposition conditions, the layers present a superhydrophobic surface, ie. a surface characterized by water drop contact angles $\theta > 150^\circ$. Such superhydrophobicity is a result of the Nafion distribution, catalyst agglomerates arrangement, and dendritic morphologies that cover the surface of the agglomerates. Superhydrophobicity extends

1
2
3
4 internally into the surface of the macropores that are formed during the electrospray process by
5
6 the sequential incorporation of ionomer and catalyst particles [11]. The result is a
7
8 *superhydrophobic porous layer* with particular properties for liquid-water transport and
9
10 interaction. One principal **property** is that the absorption of liquid water into the macropores
11
12 requires larger capillary pressures, ie. pressure difference between the liquid and the gas phases
13
14 ($p_c = p_L - p_G$), than for less hydrophobic layers; consequently, they operate under lower saturation (ie.
15
16 less liquid water occupation in the pores) in a PEMFC, where the capillary pressure is imposed by
17
18 the working conditions. In addition, liquid water tends to stay as isolated drops, instead of
19
20 continuous domains filling the pores space in **more hydrophilic** catalyst layers [12], **and,**
21
22 **preferentially, inside the larger than the smaller macropores of identical hydrophobicity [13],**
23
24 **formed during the electrospray deposition.** Such characteristics have a large impact on their
25
26 behavior as catalyst-layer because they affect water and oxygen transport [14,15]. As a result,
27
28 PEMFC with cathodic electrosprayed layers show improved performance with respect to
29
30 conventional layers, especially under high current densities, leading to peak power densities 20%
31
32 larger [10,11]. The electrosprayed layers favor highly homogeneous current distribution through
33
34 the electrode and enhance the liquid-water back-transport process, ie. water flux from the
35
36 cathode through the membrane towards the anode, keeping optimal humidification conditions in
37
38 the whole cell during operation. As a **consequence** they increase cell durability under cyclic start-
39
40 up/shut-down operation [16] or under dry gas feeds [17].
41
42
43
44
45
46
47
48
49

50 The study of mass-transport properties of superhydrophobic electrosprayed catalyst layers may
51
52 help better understand their behavior as catalyst layers, and in particular the impact of the
53
54 superhydrophobicity and related ionomer properties. In addition, electrosprayed layers may be an
55
56 option in the drive for low catalyst loadings in PEMFC electrodes, and thus lower material costs,
57
58 which appears limited by the increased gas-transport limitations at the reaction site ('local mass
59
60
61
62
63
64
65

1
2
3
4 transport resistance') [18,19,20,21]. The mass-transport resistance can be measured using
5
6 limiting-current techniques with either hydrogen or oxygen [22,23,24,25,26,27]. In the hydrogen
7
8 limiting-current technique, the GDL and catalyst-layer resistances (R_{GDL}^{mt} and R_{CL}^{mt} , respectively)
9
10 can be distinguished without the influence of water production or sluggish kinetics, and the
11
12 possibility of using D₂ and H₂ allows one to separate out the nature of the resistance [19,22].
13
14

15
16 Mass transport resistance of the catalyst layer has been analyzed with a continuum, one-
17
18 dimensional model that assumes gas-filled pores [28]. According to this model, R_{CL}^{mt} is composed
19
20 of two contributions: the 'through plane resistance', due to transport through the macro/meso
21
22 porous catalyst-layer structure in the direction perpendicular to the catalyst-layer plane; and the
23
24 'local resistance' (R_{Local}) that accounts for transport limitations very close to the reaction site. The
25
26 following mathematical expression has been obtained for R_{CL}^{mt} with the two referred terms
27
28 [27,28,29]:
29
30
31

$$R_{CL}^{mt} = \frac{L}{3D_{CL}} + \frac{R_{Local}}{\eta\gamma r_f} \quad (1)$$

32
33
34
35
36
37
38 Where L is the catalyst-layer thickness, D_{CL} is the effective reactant gas diffusion coefficient in the
39
40 pores of the inter-agglomerates space of the catalyst layer, ie. corrected for porosity (ϕ) and
41
42 tortuosity (τ) ($D_{CL} = \phi D / \tau$), r_f the catalyst roughness factor, γ (~ 0.365 for 20 wt% Pt/C particles) is
43
44 the fraction of catalyst (Pt) surface in the external surface of agglomerates (because it is the only
45
46 active under mass transport limitation) related to total catalyst surface, and η ($\sim 2-5 - 2.9$ for
47
48 ionomer thickness 5 - 10 nm) is a focusing factor that accounts for the discreteness of Pt surface
49
50 on the agglomerates. Eq.1 is able to explain the observed increase in R_{CL}^{mt} at very low loading,
51
52 which is implicit in the second term of the right.
53
54
55
56
57
58
59
60
61
62
63
64
65

1
2
3
4 In this work, R_{CL}^{mt} of electro sprayed catalyst layers is measured by the hydrogen limiting-current
5
6 technique to study their mass-transport behavior, and complemented with water-vapor uptake,
7
8 microscopy, single cell results, and impedance analysis. Transport characteristics of electro sprayed
9
10 films are compared with those of conventional airbrushed films. The results provide a more
11
12 complete picture of the behavior of electro sprayed layer and their high performance and
13
14 durability in PEMFC.
15
16
17
18

19 2. Experimental

20
21
22 Electro spray deposition of Pt/C-ionomer (Nafion) on membrane was carried out as described
23
24 elsewhere [10]. Suspensions (1 wt% solids concentration) were prepared by mixing Pt/C
25
26 commercial catalyst powder (E-TEK, 20 wt% on Vulcan XC-72R) with Nafion^R solution (Aldrich,
27
28 5wt%) in isopropanol (Panreac) solvent, and stirred in an ultrasonic bath during about 2 hours
29
30 prior to electro spray deposition. The suspension is put in a vessel under a small N₂ overpressure
31
32 (0.1-0.5 bar_g), and conducted to a metallic ejector through a silica capillary. A dc voltage (4 - 9 kV)
33
34 is imposed between the ejector (positive pole) and the substrate (negative pole) by means of a
35
36 high voltage source (Bertran, Model 205B-10R). The substrate was Nafion NRE212 (Ion Power Inc.)
37
38 with 15.2cm² active area, thermostated at 50°C, and placed on a computer controlled x-y stage.
39
40
41 Deposition was carried out in successive sweeps, at a rate of 8 μl·min⁻¹, with the suspension under
42
43 ultrasonic agitation and thermostated at 22°C. Airbrushed layers were prepared on Nafion NRE212
44
45 from suspensions of Pt/C and Nafion, using an airbrush (Vega Systems), in successive sweeps using
46
47 the same x-y stage and ink conditioning as for the electro spray deposition.
48
49
50
51
52

53
54 Single cells were mounted with the electro sprayed catalyst layer and a commercial gas diffusion
55
56 layer (GDL) (ELAT GDL LT1200W) in the cathode side. In the anode side, a commercial electrode
57
58 was used (ELAT GDE LT250EWALTSI, BASF, 0.25 mgPt·cm⁻²). Anodic and cathodic flow field plates
59
60
61
62
63
64
65

1
2
3
4 were gold plated stainless steel (Grade 310S, 2mm thickness) with double serpentine flow
5
6 channels (1mm x 1mm section). Gas tightness was accomplished with silicone gaskets. Current
7
8 collectors were gold plated brass plates, and end plates were stainless steel plates (8 mm
9
10 thickness) clamping the structure with 8 screws tightened to a controlled torque (3 N·m).
11
12
13

14 Single-cell testing was carried out using a home-made test bench, under controlled back pressure
15
16 and temperature of the cell, gases feeding through mass flow controllers, heated pipes, and
17
18 thermostated humidifiers. Cell current was drawn with an electronic load (HP 6060B), while
19
20 monitoring cell voltage and internal resistance at 1 kHz (HP Agilent 4338A milliohmmeter). Testing
21
22 followed a protocol consisting of cell start-up and heating to 80°C during first 12 hours, under a 60
23
24 mA·cm⁻² current demand; after a steady-state is attained (normally after 24 h), polarization curves
25
26 and impedance spectroscopy measurements are carried out. Polarization curves were taken at
27
28 80°C, 1 bar_g, under H₂ (Air Liquide, 99.999%) and O₂ (Air Liquide, 99.995%) flow at constant
29
30 stoichiometric factor (1.5 and 3, respectively), and 100% inlet relative humidity. Cathode
31
32 electroactive area measurements were carried out by the hydrogen underpotential deposition
33
34 method, at 30°C, and 25 mV·s⁻¹, feeding the single cell with 100% RH, H₂ in anode and N₂ in
35
36 cathode, and 40 ml·min⁻¹ flow rate. Impedance spectroscopy was taken in potentiostatic mode
37
38 superposing 10mV RMS sinusoidal voltage (Autolab 30N with 10A current booster), from 20 kHz to
39
40 0.1 Hz. The impedance spectra were analyzed using commercial software (Nova, Autolab).
41
42
43
44
45
46
47

48 For mass transport resistance measurements on electrosprayed and airbrushed catalyst layers
49
50 deposited on Nafion NRE212 membranes, the hydrogen limiting-current technique was used, as
51
52 described elsewhere [18,19,22,23]. The catalyst coated membranes were put in contact with a
53
54 Sigracet 24BC (w/ MPL & 5%PTFE) GDL as testing electrode, and an ELAT ETEK GDE as counter
55
56 electrode. Exposed electrode area was 0.713 cm². The counter electrode was fed with 2%
57
58
59
60
61
62
63
64
65

1
2
3
4 hydrogen diluted in argon, while the testing electrode was fed with 1000 ppm H₂ (or D₂) diluted in
5
6 argon with constant flow set at 200 and 500 cm³ min⁻¹ respectively, and atmospheric pressure. The
7
8 MEAs were first conditioned with 25 cyclic voltammeteries, from 0.08 to 0.95V at 50 mV s⁻¹,
9
10 followed by another 25 cleaning voltammeteries at 100 mV s⁻¹ with pure argon in the working
11
12 electrode. Before switching gases, a potential hold is applied to calculate the crossover current
13
14 values. Afterwards, limiting current (*i_{lim}*) with hydrogen and deuterium is measured recording the
15
16 current at 0.3 V after a steady state is reached. Catalyst-layer mass transport resistance (*R_{CL}^{mt}*) was
17
18 obtained from the total resistance measured (*R_{Total}^{mt}*):
19
20
21

$$R_{total}^{mt} = R_{CL}^{mt} + R_{GDL}^{mt} + R_{foil}^{mt} \quad (2)$$

22
23
24
25
26
27 Where:

$$R_{total}^{mt} = \frac{nF c_{Avg}^{Feed}}{i_{lim}} \quad (3)$$

28
29
30
31
32
33
34
35 Where *n*(=2) is the number of electrons exchanged during hydrogen oxidation (H₂ → 2H⁺ + 2e⁻),
36
37 *F*(=96485 C·mol⁻¹) the Faraday constant, *c_{Avg}^{Feed}* is the averaged reactant feed concentration in the
38
39 flow channels of the measuring cell (1000 ppm), and *i_{lim}* is the measured limiting-current density.
40
41
42 The mass-transport resistive components of the cell, ie. the gas-diffusion layer *R_{GDL}^{mt}* and the
43
44 copper foil aperture used as current collector, *R_{foil}^{mt}*, are typically < 1 s·m⁻¹, well below those of
45
46 *R_{CL}^{mt}*, so the measured mass-transport resistance can be almost entirely attributed to the catalyst
47
48 layer [29]. Each experiment was repeated at least three times, and the error determined for the
49
50 mass transport resistances is 10%, including measurements error and representative sample to
51
52 sample variability.
53
54
55

56
57 Scanning transmission electron microscopy (STEM) and electron dispersive X-ray spectroscopy
58
59 (EDS) characterization were performed for cross sectional analysis of morphology and composition
60
61

1
2
3
4 of the films [30,31]. The measurements were carried out using an FEI Talos F200X (Oregon, USA)
5
6 operated at 200kV, which is optimized for high X-ray collection efficiency by the integration of four
7
8 symmetrically arranged 30 mm² active-area silicon drift detectors within the microscope column,
9
10 resulting in a solid angle of 0.9 sr. Count-based fluorine elemental maps were acquired and were
11
12 used to examine the ionomer distribution in the CLs relative to Pt . Cross-section MEAs were
13
14 embedded in epoxy and cured at 60°C. The resulting blocks are trimmed and then sectioned into
15
16 75 nm thick cross sections by diamond knife ultramicrotomy.
17
18
19
20

21 The water uptake of the samples as a function of relative humidity (RH) and temperature was
22
23 characterized using a dynamic-vapor-sorption (DVS) analyzer (Surface Measurement Systems, UK).
24
25 With this aim, the catalyst layers were deposited by electro sprayed and airbrush deposition on
26
27 porous Teflon substrates (Whatman® TE-35 PTFE membrane filters, 0.2 μm pore size (Sigma
28
29 Aldrich), with 0.25 mg·cm⁻² platinum loading and different Nafion concentrations. **Porosity of the**
30
31 **PTFE substrate ensures that the samples have full access to the flowing humid gas, and, at the**
32
33 **same time, provides some ionic conduction necessary for electro spray deposition on non-**
34
35 **conducting substrates [10].** A sample was also prepared with carbon black (Vulcan XC-72R) and 15
36
37 wt% Nafion concentration. The samples were first equilibrated at 0% RH at 25°C for two hours to
38
39 achieve the dry state, after which the initial (dry) weight of the sample, ($M_{TFE} + M_0$) was set. The
40
41 sample was hydrated using humidified nitrogen feed to increase the RH in steps of 10% up to 90%
42
43 and then to 95% or 98%, then dehumidified back to 90% and to 0% in the same manner. The
44
45 membrane was equilibrated at each RH step for at least 1 hour or until the change in the weight
46
47 $\Delta M / (M_{PTFE} + M_0)$ was less than 0.005 %/min. In some cases, samples reached steady-state in as
48
49 little as 10 minutes. The weight of water absorbed by the sample, M_w , is determined from the
50
51 measured weight of humidified sample, M_{humid} , and its initial weight, i.e.:
52
53
54
55
56
57
58
59
60
61
62
63
64
65

$$M_W = M_{humid} - (M_{PTFE} + M_0) \quad (4)$$

Since M_W is entirely absorbed in the CL, the water fraction absorbed related to its weight is:

$$\Delta M = \frac{M_W - M_0}{M_0} \times 100. \quad (5)$$

Where the M_0 values were determined for each sample. If we assume that all the water absorbed is interacting with the ionomer sulfonic groups, then the ionomer water content, λ , which represents the number of water molecules per sulfonic-acid group of ionomer, can be calculated from:

$$\lambda = \frac{M_W / \bar{M}_W}{M_i^{dry} / EW}, \quad (6)$$

where M_i^{dry} is the dry weight of the ionomer in CL sample, EW [g/mol] is the equivalent weight of the ionomer (1100 g/mol for all samples used in this study) and \bar{M}_W is the molar weight of water (18 g·mol⁻¹). The dry weight of the ionomer is the weight fraction of ionomer, f_i , put in the catalyst layer:

$$M_i^{dry} = f_i M_0. \quad (7)$$

3. Results

3.1 Catalyst layer mass-transport resistance (R_{cl}^{mt})

The mass-transport resistance of the catalyst layers was measured for different ionomer and Pt/C concentrations, and at different gas humidities and cell temperatures. Measurements were carried out using H₂ and D₂ to probe molecular-weight specific effects on the mass transport. The results are shown in Fig. 1, together with the ratio of transport resistances with both gases, $R_{cl}^{D2} / R_{cl}^{H2}$.

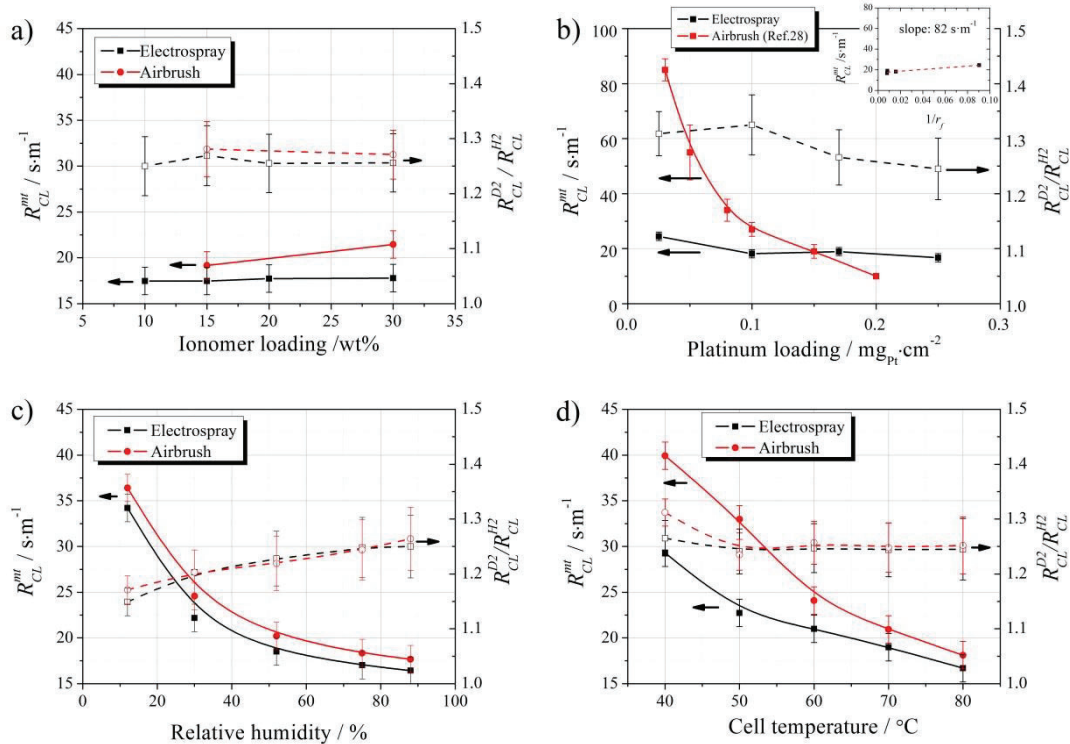


Fig.1. Mass-transport resistance (R_{CL}^{mt}), and molecular-weight specific resistances ratio (R_{CL}^{D2}/R_{CL}^{H2} , dashed line), as a function of ionomer concentration (a), Pt loading (constant Pt/C) (b), gas relative humidity (c), and cell temperature (d), for electrosprayed (black) and airbrushed (red) catalyst layers. In a) and b), measuring conditions are 80°C and 80% RH. In b), electrospayed films contain 15 wt% ionomer loading, whereas the data of airbrushed film are taken from ref.28, and correspond to films prepared with 37 wt% ionomer loading. In c) and d), the catalyst layers have 0.25 mg·cm⁻² Pt loading, and 15 wt% ionomer concentration. The inset in (b) shows the R_{CL}^{mt} vs. $1/r_f$ plot (see the text).

The electrospayed films are characterized by lower R_{CL}^{mt} , compared with airbrushed films, for all compositions and measurement conditions tested. Fig.1a shows that the ionomer concentration has minor influence on R_{CL}^{mt} of the electrospayed layers, whereas for airbrushed layers R_{CL}^{mt} increases significantly with ionomer loading. Such result indicates that the electrospay deposition

1
2
3
4 accommodates better larger amounts of the ionomer, having a minor impact on the transport
5
6 properties of the films. The same conclusion was attained from porosity measurements in a
7
8 previous work [5], and reflects an optimized distribution of the ionomer phase around the catalyst
9
10 particles as determined herein. The effect of platinum loading on R_{Cl}^{mt} of electro sprayed layers is
11
12 shown in Fig.1b. A slight increase occurs at the lowest loadings, which is less severe than the
13
14 observed in conventional layers [18,20,22,28]. In [22], an increase from $22.5 \text{ m}\cdot\text{s}^{-1}$ to $52.3 \text{ m}\cdot\text{s}^{-1}$
15
16 when decreasing loading from $0.24 \text{ mg}\cdot\text{cm}^{-2}$ to $0.028 \text{ mg}\cdot\text{cm}^{-2}$, using 40 wt% ionomer loading, was
17
18 registered for a conventional catalyst layer. The R_{Cl}^{mt} data from [28] have been included in Fig.1b
19
20 for comparison. It shows that electro sprayed films are able to better ameliorate the inherent
21
22 mass-transport losses at low Pt loadings. Such losses are mostly attributed to the local mass-
23
24 transport resistance, ie. transport losses very close to the reaction site, represented by the term
25
26 $R_{Local}/\eta\gamma$ in Eq. 1. An estimation of this term can be obtained from the slope of the linear relation
27
28 R_{Cl}^{mt} vs. $1/r_f$, as shown in the inset of Fig.1b. The value obtained, $82 \text{ s}\cdot\text{m}^{-1}$, is 20 times lower than
29
30 that measured for a conventional catalyst layer prepared with the same catalyst type (20 wt%)
31
32 [28], showing improved local mass transport in electro sprayed catalyst layers.
33
34
35
36
37
38
39

40 Fig.1 also shows the ratio of resistances using deuterium and hydrogen (R_{Cl}^{D2}/R_{Cl}^{H2}) as gas probes.
41
42 This ratio reflects the character of the transport process, approaching $R_{Cl}^{D2}/R_{Cl}^{H2} = 1.4$ for
43
44 molecular diffusive processes and decreasing when other transport processes, less dependent or
45
46 independent of the molecular weight, are limiting [22,27]. The principal molecular diffusive
47
48 processes in the catalyst layer occur for the transport of gases in the pores structure of the
49
50 catalyst layer and inside the ionomer phase, whereas other relevant processes are the interfacial
51
52 transport between the different phases present in the pores of the layer (gas, liquid, ionomer,
53
54 catalyst surface), and surface diffusion over the catalyst particle. Hydrogen transport processes
55
56 appear to be similar in electro sprayed and conventional catalyst layers in terms of dominant
57
58
59
60
61
62
63
64
65

1
2
3
4 resistance losses being about equal between molecular-weight independent and dependent
5
6 transport mechanisms. Modeling described in [28,29] allows calculating the molecular-weight-
7
8 dependent transport contribution to the transport resistance (see Supplementary Material,
9
10 Fig.S1), which shows an increasing limitation by diffusive processes at low loadings due to local
11
12 diffusion within the ionomer film. On the other hand, non-diffusive transport phenomena
13
14 increase limitation at high catalyst loadings, ascribed to transport processes through
15
16 ionomer/pore and ionomer/Pt interfaces [28].
17
18
19
20

21 Gas humidification has almost the same effect on both film types (Fig. 1c), showing a decay with
22
23 humidity that is consistent with transport through the ionomer film being the most determining
24
25 transport process. The decreasing $R_{cl}^{D_2}/R_{cl}^{H_2}$ at low humidities reflects more difficulties with
26
27 interfacial transport. However, limiting-current measurements at low RH could also be affected by
28
29 drying of the cell membrane. Cell temperature exhibits, on the other hand, different effect on
30
31 transport properties for the two catalyst layers, as shown in Fig.1d; larger slope of the airbrushed
32
33 film reflects larger thermal activation of transport than in electrospayed films, especially at low
34
35 temperature (< 50°C). Similar $R_{cl}^{D_2}/R_{cl}^{H_2}$ in both layer types demonstrates that the controlling
36
37 transport processes must be qualitatively similar in both catalyst-layer types, with some more
38
39 differences at the lowest temperature (40°C). The larger thermal activation of the airbrushed
40
41 layer may be a consequence of its lower water-vapor-uptake capability (see below), which
42
43 determines hydrogen transport within the ionomer film.
44
45
46
47
48
49
50
51
52
53
54
55
56
57
58
59
60
61
62
63
64
65

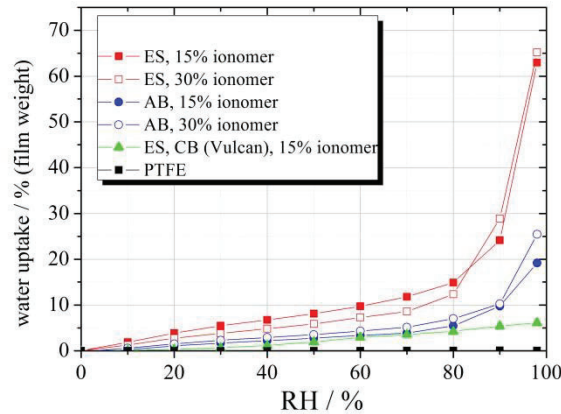


Fig. 2. Water-vapor uptake desorption curves (see Supplementary Material, Fig. S2, for absorption curves and results of λ calculation), as a function of relative humidity, for catalyst layers deposited by electro spray and airbrushing. Results for the PTFE substrate are also included.

Water-vapor uptake measurements on catalyst layers prepared by electro spray and airbrushing are shown in Fig. 2. In these experiments, water vapor enters the macropores structure of the CL leading to a mass increase upon absorption/adsorption into the layer [32]. We notice in Fig.2a that the electro spray catalyst layer is characterized by larger water-vapor-uptake capacity than the airbrushed layers in the whole range of relative humidities. Such a result may explain partially their lower R_{CL}^{mt} due to better ionomer hydration (Fig.1c), and the good behavior that they show in fuel-cell operation under low humidification conditions [17]. Assuming that all water vapor absorbs into the ionomer, the water content λ can be calculated from Eq. 6; the result and comments are included in the Supplementary Information together with the absorption curves (Fig. S2). The data in Fig.2 also confirm that Pt plays a critical role in orientating the ionomer chains or perhaps concentrating them (see STEM data below), thereby resulting a much lower water uptake for only C containing layers, which is consistent with prior studies [32]. The time dependent water-uptake fraction, taken during the measurements in Fig.2, show higher rate for

1
2
3
4 water absorption in the electro sprayed film than in the airbrushed film, especially at low ionomer
5
6 loading, which is a clear indication of the favored conditions for water-vapor interaction leading to
7
8 larger water-vapor uptake capability (see Supplementary Information, Fig.S3).
9

10
11 It must be noted that the enhanced water-vapor uptake of the electro sprayed layers is
12
13 accompanied by very low wettability and superhydrophobic character [11,16,Error! Bookmark not
14
15 defined.33,34]. Such apparently opposite properties must be a consequence of the catalyst layer
16
17 and ionomer phase resulting from the electro spray deposition, with macropores walls containing
18
19 dendritic structures that decrease the adhesion of liquid water, combined with the ionomer
20
21 closely interacting with the platinum surface with enhanced reactivity with water vapor molecules
22
23 (see Discussion). They also explain the capability for fast water transport while retaining high ionic
24
25 conductivity, which is most appropriate for a catalyst layer in a PEMFC.
26
27
28
29
30

31 32 3.2 Cross sectional morphology under STEM

33
34
35 Information about morphology and components distribution in electro sprayed catalyst layers can
36
37 be obtained from cross sectional STEM images. Fig. 3 shows images of a catalyst layer with a Pt
38
39 load of $0.025 \text{ mg}\cdot\text{cm}^{-2}$ and an ionomer loading of 15 wt.% (respect to the total layer weight),
40
41 deposited on Nafion NR212.
42
43
44
45
46
47
48
49
50
51
52
53
54
55
56
57
58
59
60
61
62
63
64
65

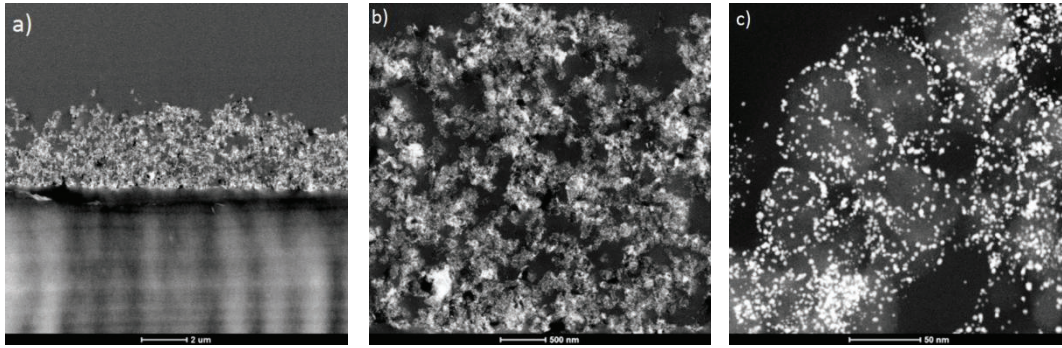


Fig.3. STEM images in cross section of an electro sprayed Pt/C + ionomer layer ($0.025 \text{ mg}\cdot\text{cm}^{-2}$, 15 wt% ionomer), at three different magnifications.

At lower magnification (Fig.3a) the layer shows irregular thickness, 3 to 4 μm , with large macropores ($> 50 \text{ nm}$). At higher magnification (Fig.3b,c), the Pt catalyst nanoparticles appear evenly distributed showing no alteration at this level by the electro spray process [4].

The distribution of elements Pt, F, and C in the catalyst layer is shown in Fig.4. The STEM image shows Pt and carbon black phases (Fig.4a) that closely follow the contrasts of the Pt image (Fig. 4b) and the C image (Fig. 4c), respectively, as expected. Most significant in Fig.4 is the similarity between the distribution of Pt and F (cf Figs. 4b and c) in most areas (see the area inside the circle for example), that reflects a preferential interaction of the Nafion ionomer with Pt nanoparticles, and less with C support. Previous evidences of a specific interaction of the ionomer with Pt in electro sprayed films were obtained from thermogravimetric analysis [4]. STEM images of layers prepared with a common spray technique show, on the other hand, the ionomer covering uniformly all the surface of the particles [35].

1
2
3
4
5
6
7
8
9
10
11
12
13
14
15
16
17
18
19
20
21
22
23
24
25
26
27
28
29
30
31
32
33
34
35
36
37
38
39
40
41
42
43
44
45
46
47
48
49
50
51
52
53
54
55
56
57
58
59
60
61
62
63
64
65

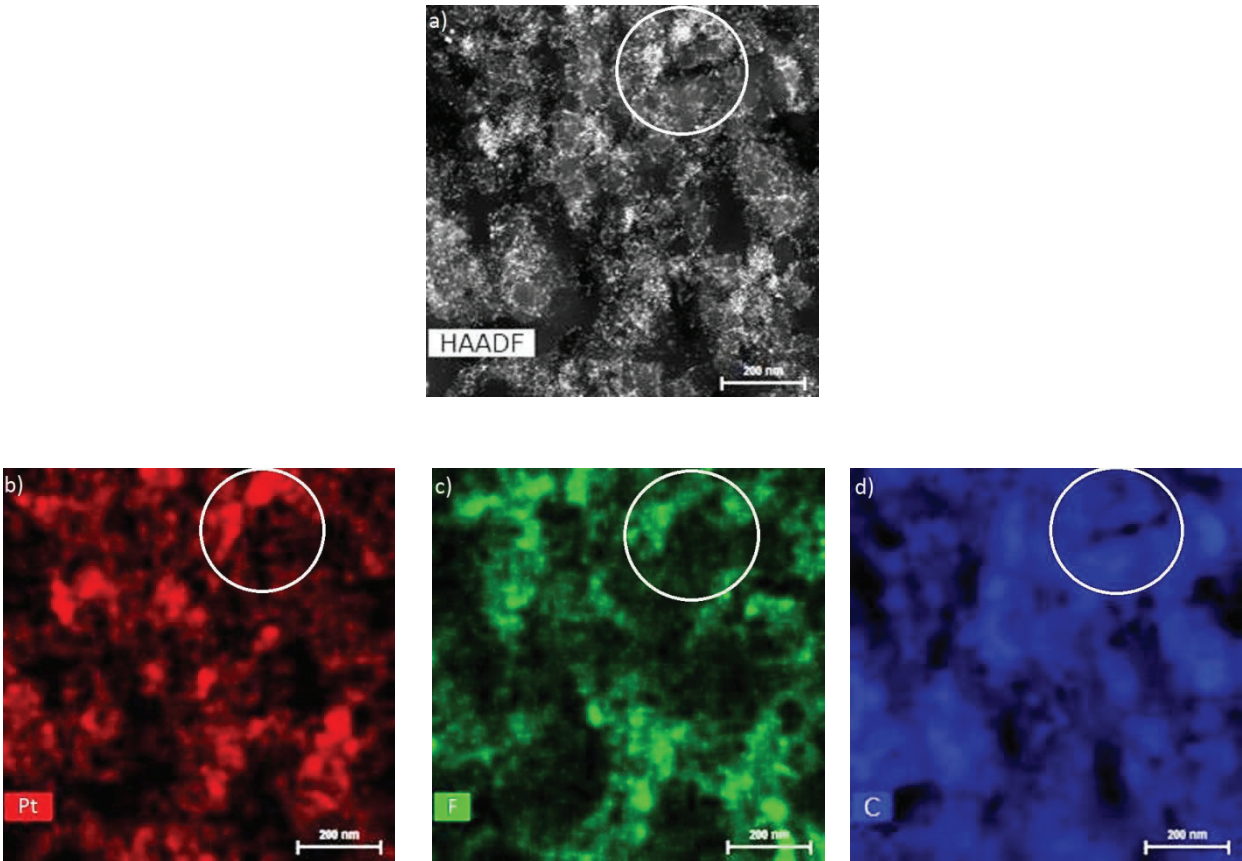


Fig.4. High-angle annular dark-field STEM image (a), and images of the distribution of Pt (b), F (c), and C (d). Circle for visual guide.

3.3 Single-cell testing

Single cells were mounted with electrospayed catalyst layers in the cathodic electrode. Polarization curves and power density are shown in Fig.5, for four layers with different catalyst loadings.

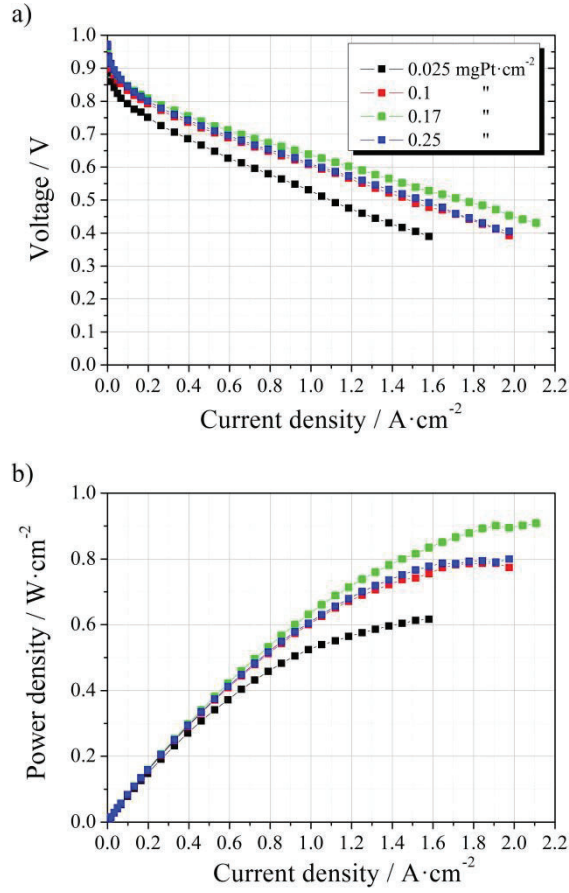


Fig.5. a) Polarization curves of single PEMFCs with electro sprayed catalyst layers of variable Pt loading in the cathode. b) Power density curves. Cells were tested at 80 °C, 1 bar_g, and 100% RH conditions, using H₂/O₂ (1.5/3.0 stoichiometry) in anode/cathode. Polarization curves at 0% RH are shown in Supplementary Material, Fig.S5.

An optimal cell response is attained at a cathode loading of 0.17 mg_{pt}·cm⁻² in accordance with previous results [36]. The curves were analyzed using a simple 0-D equation:

$$V = E' - b \cdot \log \frac{j}{r_f \cdot j_0} - j \cdot R_i^{dc} \quad (8)$$

Where V is the cell voltage, E' is the thermodynamic potential, b is the Tafel slope, j the current density, j_0 the exchange current density per unit platinum area ($j_0 = 8.5 \cdot 10^{-9}$ A·cm⁻²_{pt}, [37]), r_f

($\text{cm}^2_{\text{Pt}} \cdot \text{cm}^{-2}$) the roughness factor, and R_i^{dc} the dc internal resistance. The roughness factor was obtained from the measured electrochemical area ($r_f = L_{\text{Pt}} A_{\text{Pt}}$, where L_{Pt} is the platinum loading). Both, r_f and A_{Pt} , are plotted in Fig.6a as a function of platinum loading.

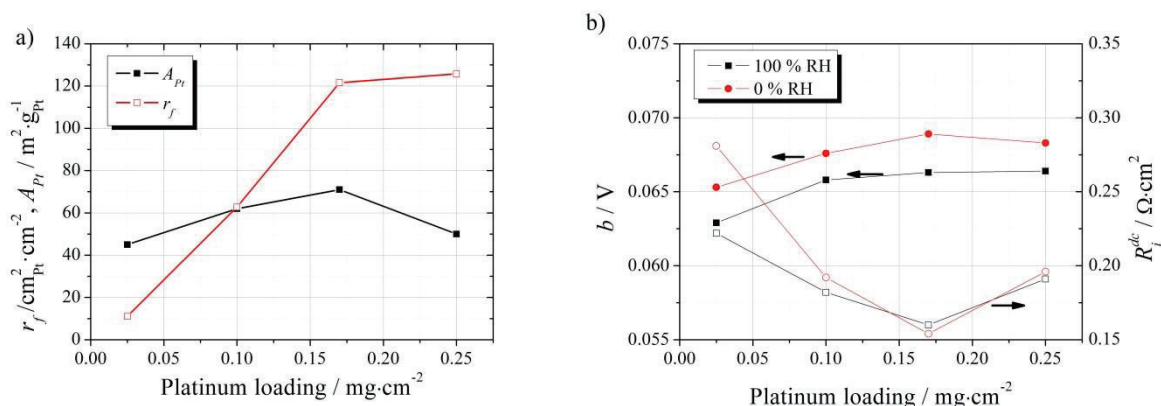


Fig. 6.- a) Roughness factor (r_f) and mass specific electrochemical area (A_{Pt}) of the electrospayed catalyst layers of Fig.5 as a function of Pt loading. b) Tafel slope (b) and dc internal resistance (R_i^{dc}) at 100% RH and 0% RH, obtained from the least square fitting of polarization curves in Fig.5 to Eq.8.

A peak in the mass-specific Pt area is encountered at $0.17 \text{ mg}_{\text{Pt}} \cdot \text{cm}^{-2}$, which reflects the conditions for the maximum accessibility of the platinum surface to reactants, which agrees with the maximum response in the polarization curves of Fig.5. A plateau in r_f and decrease in A_{Pt} at larger loadings (Fig.6a) is consistent with additional Pt being less accessible, although mass-transport is not worsen, as shown by the leveling of R_{CL}^{mt} at higher loadings in Fig.1b.

Results of the least-square-fitting analysis of polarization curves to Eq.8 are in Fig. 6b, where b and R_i^{dc} are plotted as a function of platinum loading, at 0% RH and 100% RH (Polarization curves at 0% RH are in Supplemental Material, Fig. S5). For the fitting only points below $0.8 \text{ A} \cdot \text{cm}^{-2}$ were considered to assure full catalyst layer limitation conditions (charge transfer and mass transport)

1
2
3
4 and without any other external mass transport limitation, as implicit in Eq.8 where the mass
5
6 transport limitation term has been drop. According to the simple model used, parameter b gathers
7
8 polarization losses in the catalyst layer, either due to kinetics, ohmic, or mass transport. The
9
10 increase in b with catalyst loading must be attributed to ohmic losses occurring by the increasing
11
12 thickness of the catalyst layer (thicknesses are provided in Supplementary Material, Fig.S4). The
13
14 increase in Tafel slope with thickness of the catalyst layer, keeping constant the Pt loading, was
15
16 encountered by M. Lee et al. in spray-coated membranes with variable Pt/C ratio [38], and T.
17
18 Suzuki et al. [39] in coated membranes prepared with a doctor blade technique and blending Pt/C
19
20 particles with stand-alone carbon black. The larger b registered at 0% RH than at 100% RH in Fig.6b
21
22 could indicate either a decrease in catalyst performance, since liquid water in the catalyst layer
23
24 favors the electrocatalysis of the oxygen reduction reaction [11,40], and/or additional mass
25
26 transport losses at low RH and shifting of the reaction distribution next to the membrane. Most
27
28 determining for fuel cell response, however, appears to be the evolution of R_i^{dc} in Fig. 6b. As a
29
30 difference from the results of Tafel slopes, internal resistance shows almost no differences
31
32 between 0% and 100% RH (except at the lowest loading), which is due to the electrospayed
33
34 catalyst layer keeping similar fuel cell performance under low humidity [17] (see also Fig.S5 in
35
36 Supplementary Material). The minimum R_i^{dc} at $0.17 \text{ mg}_{\text{Pt}} \cdot \text{cm}^{-2}$ correlates with the maxima in A_{Pt}
37
38 (Fig.6a) and cell performance (Fig.5). At this loading, conditions are optimal for the transport of
39
40 gases, ionic conduction, and for Pt catalyst utilization in the electrospayed cathodic catalyst layer,
41
42 which are a consequence of its high water-vapor uptake capability and superhydrophobic
43
44 character. More insight into the transport properties of the electrospayed layers can be obtained
45
46 from the impedance spectroscopy analysis.
47
48
49
50
51
52
53
54
55
56
57
58
59
60
61
62
63
64
65

3.4 Electrochemical impedance spectroscopy

Impedance spectroscopy was carried out on the cells with electro sprayed cathode catalyst layer. Nyquist plots exhibit one unique semicircle response at cell voltages between 0.8 and 0.6V (see Supplementary Material, Fig.S6), that is entirely ascribed to the catalyst layer impedance [41]. A second semicircle at low frequencies, reflecting transport losses in other parts of the cell, like the gas diffusion layers or the flow fields, is not observed at these cell voltages and operating conditions. The results of the analysis are shown in Fig.7, using the electrical circuit in the inset, where the series resistance element (R_s) accounts for the fast ohmic losses due to ionic conduction in the membrane and electronic conduction in the electrodes and contacts, R_{CL} accounts for transport and charge transfer losses in the cathodic catalyst layer, and the constant phase element (Y_{CL}, n) is related with the pseudo-capacitive character of this same layer [42].

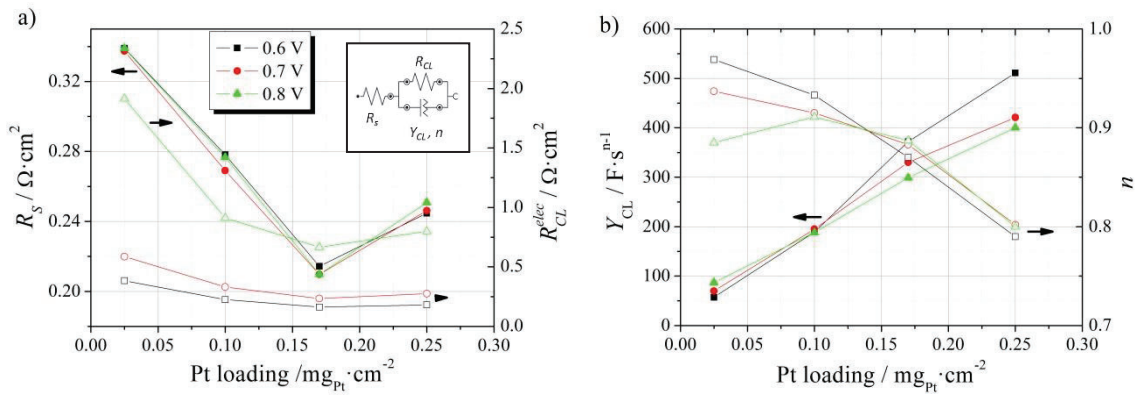


Fig.7. a) Series resistance (R_s , full symbols) and catalyst layer resistance (R_{CL} , open symbols) as a function of Pt loading in the electro sprayed catalyst layer, at three cell voltages. b) Constant phase element parameters, Y_{CL} (full symbols) and n (open symbols), as a function of catalyst loading, at three cell voltages. Inset in a) shows the electric circuit used for the impedance analysis. Cell conditions as in Fig. 5.

1
2
3
4 Cell series (R_s) and catalyst-layer (R_{CL}) resistances are plotted in Fig.7a as a function of catalyst
5
6 loading for three cell voltages. The minimum in R_s at $0.17 \text{ mg}\cdot\text{cm}^{-2}$ is concomitant with the general
7
8 optimization of cell parameters, ie. the minimum in R_i^{dc} (Fig. 6b) and the maximum A_{Pt} (Figs. 6b),
9
10 and cell response in Fig. 5. In this case it shows that the ionic conduction in the cell is optimal at
11
12 this loading. Fig. 7a shows also a minimum in R_{CL} at the same Pt loading, more pronounced at high
13
14 cell potential (low overpotentials) when the cathode catalyst-layer properties govern the cell
15
16 response. Such minimum reflects the optimization of the electrochemical kinetics and mass
17
18 transport in the cathodic catalyst layer.
19
20
21

22
23
24 The analysis of the constant-phase-element parameters in Fig.7b provides some more useful
25
26 information about the behavior of the electrosprayed catalyst layers. Parameter n of this circuit
27
28 element reflects the dispersion of time constants frequently encountered in solid electrodes, with
29
30 $n=1$ for the case of a single time constant, and decreasing ($0 < n < 1$) by increasing dispersion [42].
31
32 For a catalyst layer, dispersion may be larger by increasing the layer thickness because of larger
33
34 heterogeneities in all parameters affecting its response, e.g., temperature, pressure, potential,
35
36 current, concentration of reactants, water, etc. Consequently, results in Fig. 7b show that n
37
38 decreases with catalyst loading (film thickness). On the other hand, Y_{CL} shows a continuous
39
40 increase with the platinum loading, with increasing slope by decreasing cell voltage (increasing the
41
42 current). The information of interest from this parameter resides in its pseudo-capacitive
43
44 character which is related with charge storage in the catalyst layer. A capacitance can be
45
46 determined from Y_{CL} using the following relationship [42,43]:
47
48
49
50
51
52

$$53 \quad C_{CL} = Y_{CL}^{1/n} R_{CL}^{(\frac{1}{n}-1)} \quad (9)$$

54
55
56
57 Where C_{CL} is the electrical capacitance of the cathodic catalyst layer. The result of the conversion is
58
59 plotted in Fig.8. A capacitance peak with loading is found at $0.17 \text{ mg}_{Pt}\cdot\text{cm}^{-2}$ ($0.68 \text{ mg}_C\cdot\text{cm}^{-2}$), which
60
61

shows similar dependence as the electrochemical active platinum area in Fig.6a, although C_{CL} must be related with the whole electrochemical active area of the catalyst layer, ie. C and Pt surfaces (in fact Pt surface has minor contribution compared with carbon black). Fig, 7c includes the nominal capacitance expected for the carbon black surface, taking specific area $210 \text{ m}^2 \cdot \text{g}_C^{-1}$ and specific capacitance $16 \mu\text{F} \cdot \text{cm}^{-2}$ [44], that shows good agreement with the experimental curves only at low loadings. The saturation of the charge storage, together with that observed for the electrocatalyst surface (Fig.6a), indicate that above $0.17 \text{ mg}_{\text{Pt}} \cdot \text{cm}^{-2}$ the additional electrospayed catalyst layer is electrochemically inactive. Such result may be a consequence of the water transport and wetting properties of superhydrophobic catalyst layers, as explained in the following section.

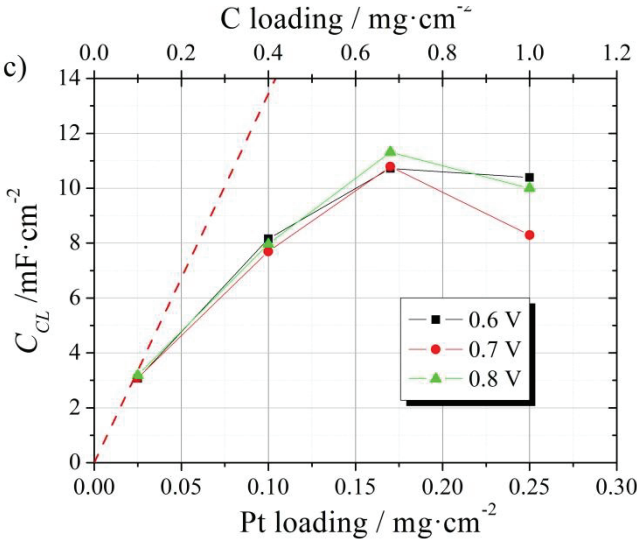


Fig.8. Result of the application of Eq.9 to impedance analysis in Fig. 7b. Dashed red line indicates the estimated nominal capacitance of the carbon black phase.

4. Discussion

Mass transport in electro sprayed catalyst layers is characterized by lower R_{Cl}^{mt} values compared with conventional airbrushed layers, up to 25% lower depending on composition and testing conditions. The differences are more important in layers with low platinum loading (Fig. 1b) and at low temperatures (Fig.1d). It is also significant that a low impact on transport resistance is witnessed with ionomer concentration (Fig.1a), which appears to interact preferentially with the Pt phase in the elemental mappings of Pt and F (Fig. 4). Water-vapor uptake capability of electro sprayed catalyst layers is higher than conventional layers (Fig.2, and see also Fig.S2 in [Supplementary Material](#)). This reflects that the nanostructure and distribution resulting from the electro sprayed deposition, including the enhanced interaction with Pt, which itself has an important effect on water-vapor uptake, result in an ionomer that more readily absorbs water, and thus exhibits better transport properties. This characteristic is in stark contrast with the superhydrophobicity of electro spray catalyst layers, which show very high liquid water contact angles, above 150° , and low wettability [11,16,17]. Both properties must be a result of a macroporous catalyst layer with highly available hydrophilic groups (sulfonic groups of the ionomer) inside a pore structure which walls, having dendrite growths of the catalyst particles and the ionomer, favor air trapped pockets and preclude liquid-water interaction, like in a Cassie state surface [45]. The combined high water-vapor absorption with superhydrophobicity optimizes the function of a PEMFC catalyst layer under different operation conditions since it provides good ionic conductivity along with superior liquid-water transport characteristics.

The expected enhancement from the ex-situ analysis is observed in single cell testing, where an optimal electro sprayed loading occurs at $0.17 \text{ mg}\cdot\text{cm}^{-2}$ (using catalyst Pt/C 20wt%) in accordance with that found in previous studies [36], and which corresponds with a layer thickness of $18 \mu\text{m}$

1
2
3
4 (see Supplementary Material, Fig.S4). At this loading, the highest active areas are measured for
5
6 the Pt surface catalyst and for the carbon surface (Figs.6a and 8, respectively), the second one
7
8 inferred from larger double-layer capacitance. Also, at this loading, all ohmic resistances (
9
10 electronic and ionic) are minimized (Fig. 6b).

11
12
13
14 The experimental mass transport (R_{CL}^{mt}) is a contribution to the catalyst layer resistance (R_{CL}). A
15
16 simplified picture can be used that considers the second one as composed of three serial
17
18 contributions:
19
20

$$21 \quad R_{CL} = R_{CL}^{kin} + R_{CL}^{ohm} + f \cdot R_{CL}^{mt} \quad (10)$$

22
23
24
25 Where R_{CL}^{kin} is the kinetic resistance (charge transfer), and R_{CL}^{ohm} is the ohmic resistance due to
26
27 protonic and electronic conduction in the catalyst layer ($R_{CL}^{ohm} = R_{CL}^{ohm,H^+} + R_{CL}^{ohm,e^-}$); f ($V \text{ cm}^3 \text{ C}^{-1}$) is a
28
29 proportionality factor that takes into account oxygen parameters (molecular weight, n , and
30
31 concentration) and the change of units. Eq. 10 helps to rationalize the results of mass transport
32
33 and impedance. The increase in R_{CL} at low loading can be attributed to R_{CL}^{mt} , ie. the local mass
34
35 transport resistance, and also R_{CL}^{kin} contributes due to the low loading. Other characteristics of the
36
37 impedance results require considering additional effects. The increase in R_s at low loadings
38
39 (Fig.7a), which must be related with R_{CL}^{ohm} in Eq.10, reflects a decrease in the electronic or ionic
40
41 conduction of the catalyst layer; in addition, the slight increase in R_{CL} at high loadings (Fig.7a)
42
43 cannot be a mass transport effect because R_{CL}^{mt} decreases in the loading range studied here (Fig.
44
45
46
47
48
49
50
51
52
53
54
55
56
57
58
59
60
61
62
63
64
65

66
67
68
69
70
71
72
73
74
75
76
77
78
79
80
81
82
83
84
85
86
87
88
89
90
91
92
93
94
95
96
97
98
99
100

1
2
3
4 behavior can only be explained as a consequence of particular wetting properties of the
5
6 superhydrophobic 'thin porous film' having a thickness lower or comparable with their
7
8 characteristic pores size. It is known that thin porous films have different properties than thicker
9
10 ones, like permeability, wetting, and water transport [46]. On this ground, an explanation can be
11
12 proposed for the trends observed in the impedance response and mass transport of the
13
14 electrospayed catalyst layers (cf. Fig S7 in Supplementary Material). At very low thickness, the
15
16 thin porous layer in contact with the fully humidified PEM is flooded because no capillary pressure
17
18 is developed to repeal the liquid water of the PEM, so water invasion occurs. Therefore, very thin
19
20 catalyst-layers are characterised by high R_{CL}^{mt} ('through plane' resistances term in Eq.1) and
21
22 R_{CL}^{ohm,e^-} (electronic resistance component due to loss of inter-particles contact in a flooded layer).
23
24 Increasing catalyst-layer thickness makes possible capillary forces to decrease liquid water
25
26 saturation and a decrease in R_{CL}^{mt} and R_{CL}^{ohm} is observed (Figs.1b and 7a), up to a certain
27
28 thickness where the superhydrophobic catalyst layer impose too dry conditions which increases
29
30 the protonic resistance (R_{CL}^{ohm,H^+}) and decreases catalyst utilization (Fig.6a). There is, therefore, an
31
32 optimal thickness that allows for mixed wettability and partially saturated layer, leading to the
33
34 lowest mass transport, electronic, and protonic resistances, and maximum Pt utilization. For the
35
36 case of electrospayed films with Pt/C 20wt% the thickness is 18 μm ($0.17 \text{ mg}_{\text{Pt}} \cdot \text{cm}^{-2}$). Decreasing
37
38 the optimal catalyst loading, therefore, requires maintaining the optimal thickness in order to
39
40 avoid flooding in too thin layers. In the Supplementary Material, Fig.S7, a scheme depicts
41
42 schematically the three characteristics saturation states for a superhydrophobic catalyst layer in
43
44 dependence of thickness.
45
46
47
48
49
50
51
52
53
54
55
56
57
58
59
60
61
62
63
64
65

1
2
3
4 **5. Conclusions**
5
6

7 Transport properties of catalyst layers prepared by electrospray deposition have been studied by
8 mass-transport-resistance measurements and correlated with water-vapor uptake, ionomer phase
9 distribution imaging, and single-cell performance. The following conclusions have been obtained
10 from the study:
11
12

13
14
15
16
17
18 - Low mass transport resistance reveals improved transport properties of electrosprayed catalyst
19 layers compared with conventional layers.
20

21
22
23 - Water-vapor uptake is larger for electrosprayed layer that we attribute to the particular
24 morphology and distribution of the ionomer phase, which shows a specific interaction with the
25 platinum surface.
26
27

28
29
30
31 - The enhanced water-vapor uptake of electrosprayed layers combined with their very low
32 wettability and superhydrophobic character, studied in previous works, allow for an optimal
33 catalyst layer with low mass transport resistance and high ionic conductivity.
34
35

36
37
38
39 - Single cell results reveal an optimal Pt loading of $0.17 \text{ mgPt}\cdot\text{cm}^{-2}$ for electrosprayed layers
40 prepared with Pt/C 20wt% catalyst, that correspond to the thickness of $18 \mu\text{m}$. Such layer allows
41 for optimal mass transport, catalyst utilization, and ionic conductivity. Decreasing the optimal
42 loading requires keeping similar catalyst layer thickness to avoid local mass transport losses and
43 flooding that occurs in too thin layers.
44
45
46
47
48
49

50
51
52 **Acknowledgements**
53

54
55 This work was supported by the Ministerio de Economía y Competitividad of Spain, and Fondo
56 Europeo de Desarrollo Regional (FEDER), Project E-LIG-E, ENE2015-70417-P (MINECO/FEDER).
57
58

1
2
3
4
5
6
7
8
9
10
11
12
13
14
15
16
17
18
19
20
21
22
23
24
25
26
27
28
29
30
31
32
33
34
35
36
37
38
39
40
41
42
43
44
45
46
47
48
49
50
51
52
53
54
55
56
57
58
59
60
61
62
63
64
65

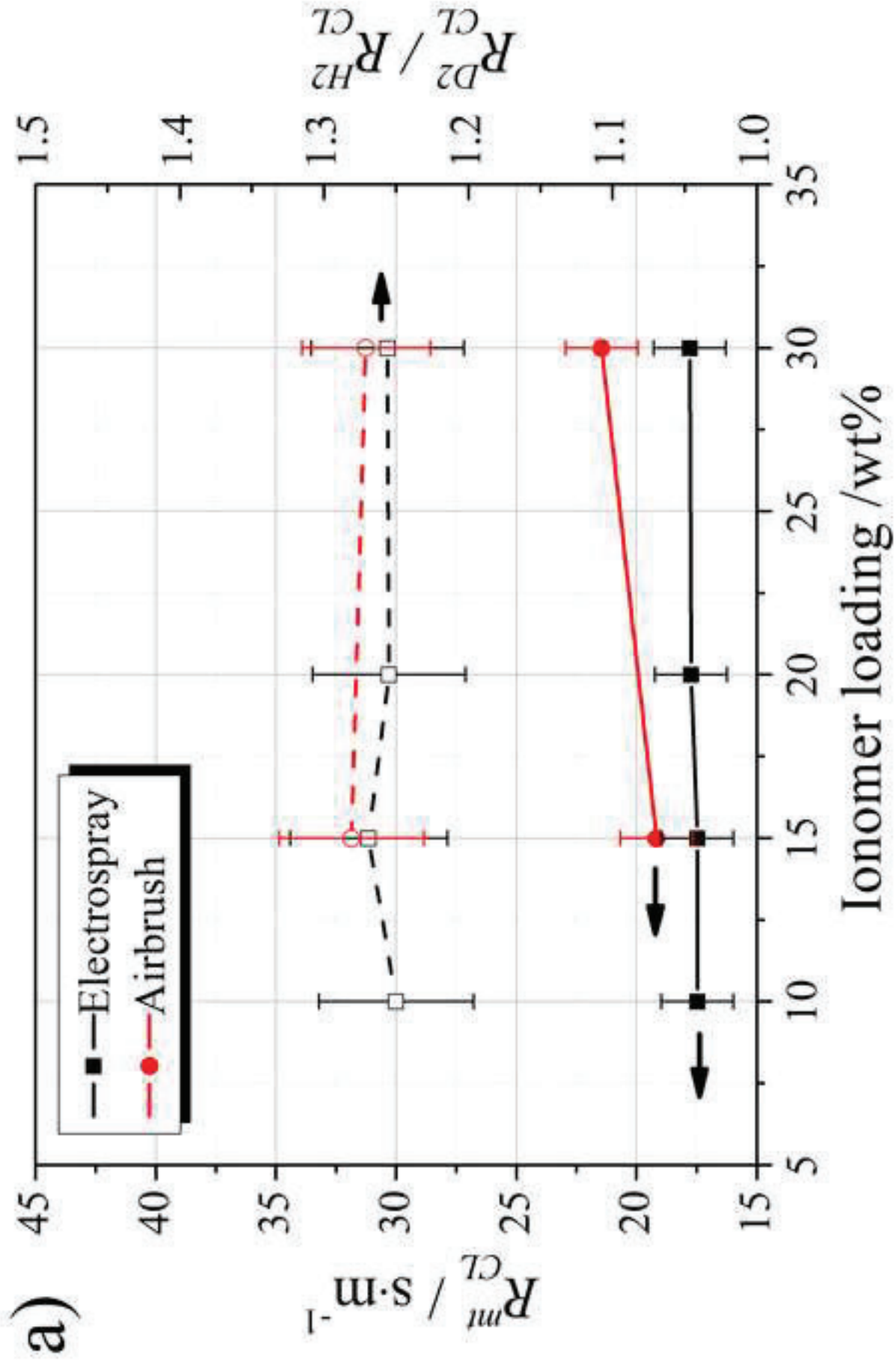
Microscopy conducted at ORNL’s Center for Nanophase Materials Sciences, which is a U.S. DOE Office of Science User Facility. LBNL and ORNL research was supported by the Fuel Cell Technologies Office, Office of Energy Efficiency and Renewable Energy, U.S. DOE, and was conducted through the FC-PAD Consortium.

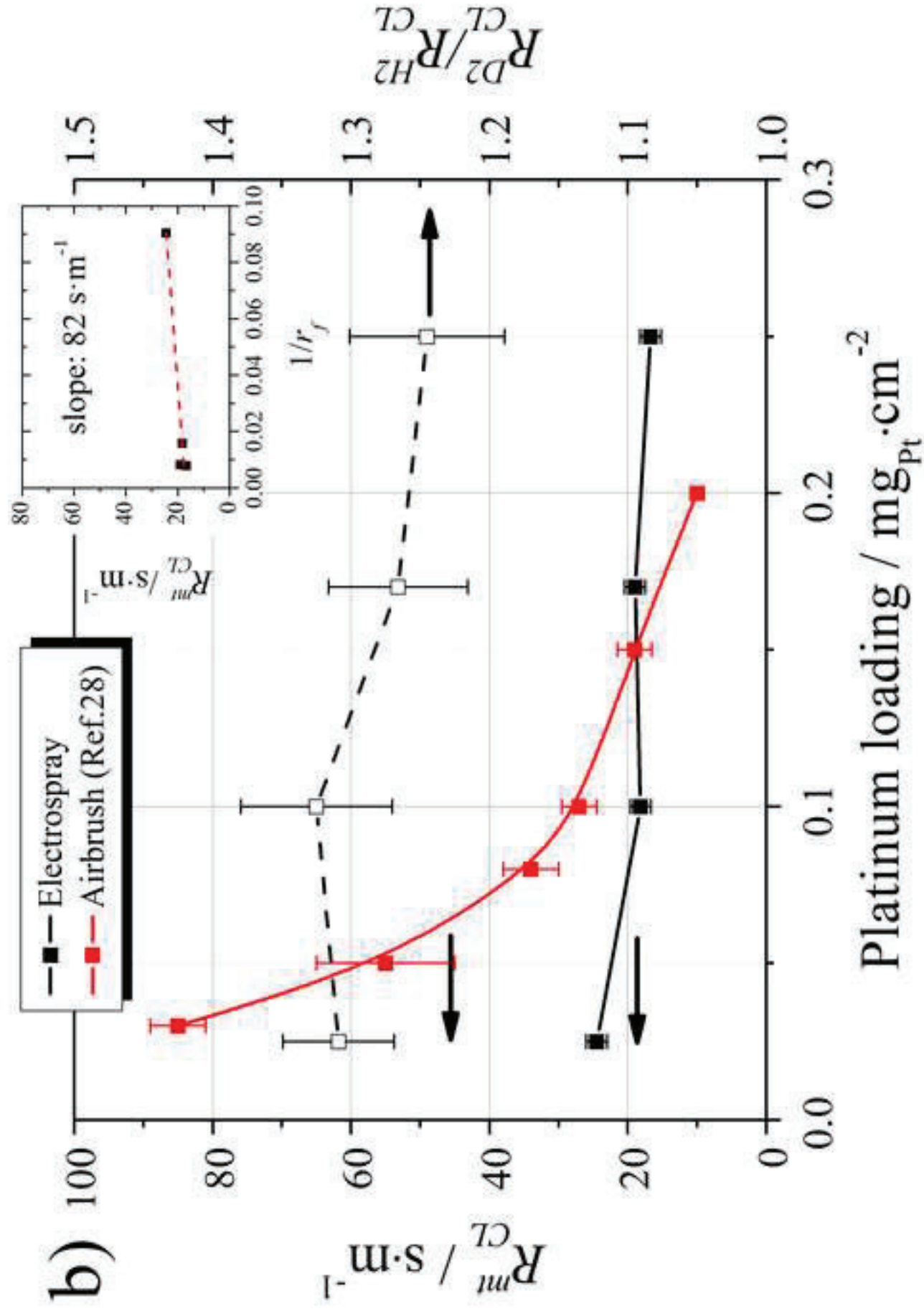
1
2
3
4
5
6
7 **References**
8

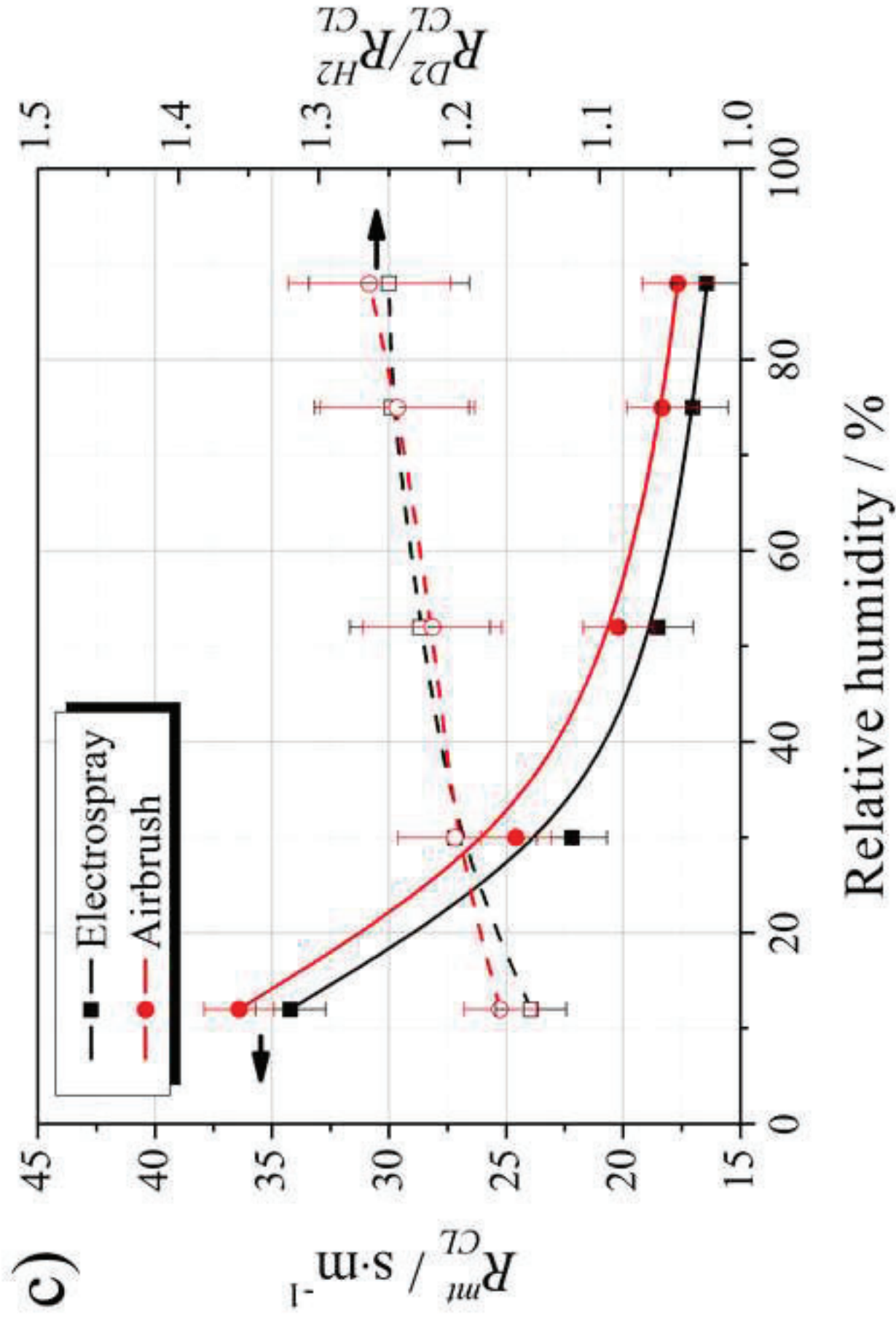
- 9 [1] T.E. Springer, T.A. Zawodzinski, S. Gottesfeld, Polymer Electrolyte Fuel Cell Model, *J. Electrochem. Soc.* 138 (1991) 2334-2342. <https://doi.org/10.1149/1.2085971>
10
11
12 [2] A.Z. Weber, J. Newman, Modeling Transport in Polymer-Electrolyte Fuel Cells, *Chem. Rev.* 104 (2004) 4679-4726.
13
14
15 [3] S. Litster, G. McLean, PEM fuel cell electrodes, *J. Power Sources* 130 (2004) 61–76.
16
17 [4] A.M. Chaparro, R. Benítez, L. Gubler, G.G. Scherer, L. Daza, Study of membrane electrode assemblies for
18 PEMFC with cathodes prepared by the electrospray method, *J. Power Sources* 169 (2007) 77–84.
19
20 [5] A. M. Chaparro, M. A. Folgado, P. Ferreira-Aparicio, A. J. Martín, I. Alonso-Álvarez, L. Daza, Properties of
21 Catalyst Layers for PEMFC Electrodes Prepared by Electrospray Deposition, *J. Electrochem. Soc.* 157 (2010)
22 B993-B999.
23
24 [6] S. Martin, P. L. Garcia-Ybarra, J. L. Castillo, High platinum utilization in ultra-low Pt loaded PEM fuel cell
25 cathodes prepared by electrospraying, *Int. J. Hydrogen Ener.* 35 (2010) 10446-10451.
26
27 [7] K. Takahashi, K. Kakinuma, M. Uchida, Improvement of Cell Performance in Low-Pt-Loading PEFC
28 Cathode Catalyst Layers Prepared by the Electrospray Method, *J. Electrochem. Soc.* 163 (2016) F1182-F1188.
29
30 [8] B-S. Koh, J-H. Yoo, E-K Jang, V. R. Jothi, C-Y. Jung, S.C. Yi, Fabrication of highly effective self-humidifying
31 membrane electrode assembly for proton exchange membrane fuel cells via electrostatic spray deposition,
32 *Electrochem. Comm.* 93 (2018) 76–80.
33
34 [9] N. Chingthamai, K. Sombatmankhong, Y. Laoonual, Experimental investigation of electrospray coating
35 technique for electrode fabrication in PEMFCs, *Energy Procedia* 105 (2017) 1806 – 1812.
36
37 [10] A.M. Chaparro, P. Ferreira-Aparicio, M.A. Folgado, A.J. Martín, L. Daza, Catalyst layers for proton
38 exchange membrane fuel cells prepared by electrospray deposition on Nafion membrane, *J. Power Sources*
39 196 (2011) 4200–4208.
40
41 [11] A.M. Chaparro, P. Ferreira-Aparicio, M.A. Folgado, E. Brightman, G. Hinds, Study of superhydrophobic
42 electrosprayed catalyst layers using a localized reference electrode technique, *J. Power Sources* 325 (2016)
43 609-619.
44
45 [12] J. Bear, *Dynamics of Fluids in Porous Media*, Dover Publications, Inc., New York, 1988.
46
47 [13] T. Hutzenlaub, J. Becker, R. Zengerle, S. Thiele, Modelling the water distribution within a hydrophilic and
48 hydrophobic 3D reconstructed cathode catalyst layer of a proton exchange membrane fuel cell, *J. Power*
49 *Sources* 227 (2013) 260-266.
50
51 [14] X. Wang, T. Van Nguyen, Modeling the Effects of Capillary Property of Porous Media on the
52 Performance of the Cathode of a PEMFC, *J. Electrochem. Soc.* 155 (2008) B1085-B1092.
53
54 [15] M. El Hannach, M. Prat, J. Pauchet, Pore network model of the cathode catalyst layer of proton
55 exchange membrane fuel cells: Analysis of water management and electrical performance, *Int. J. Hydrogen*
56 *Ener.* 37 (2012) 18996-19006.
57
58
59
60
61
62
63
64
65

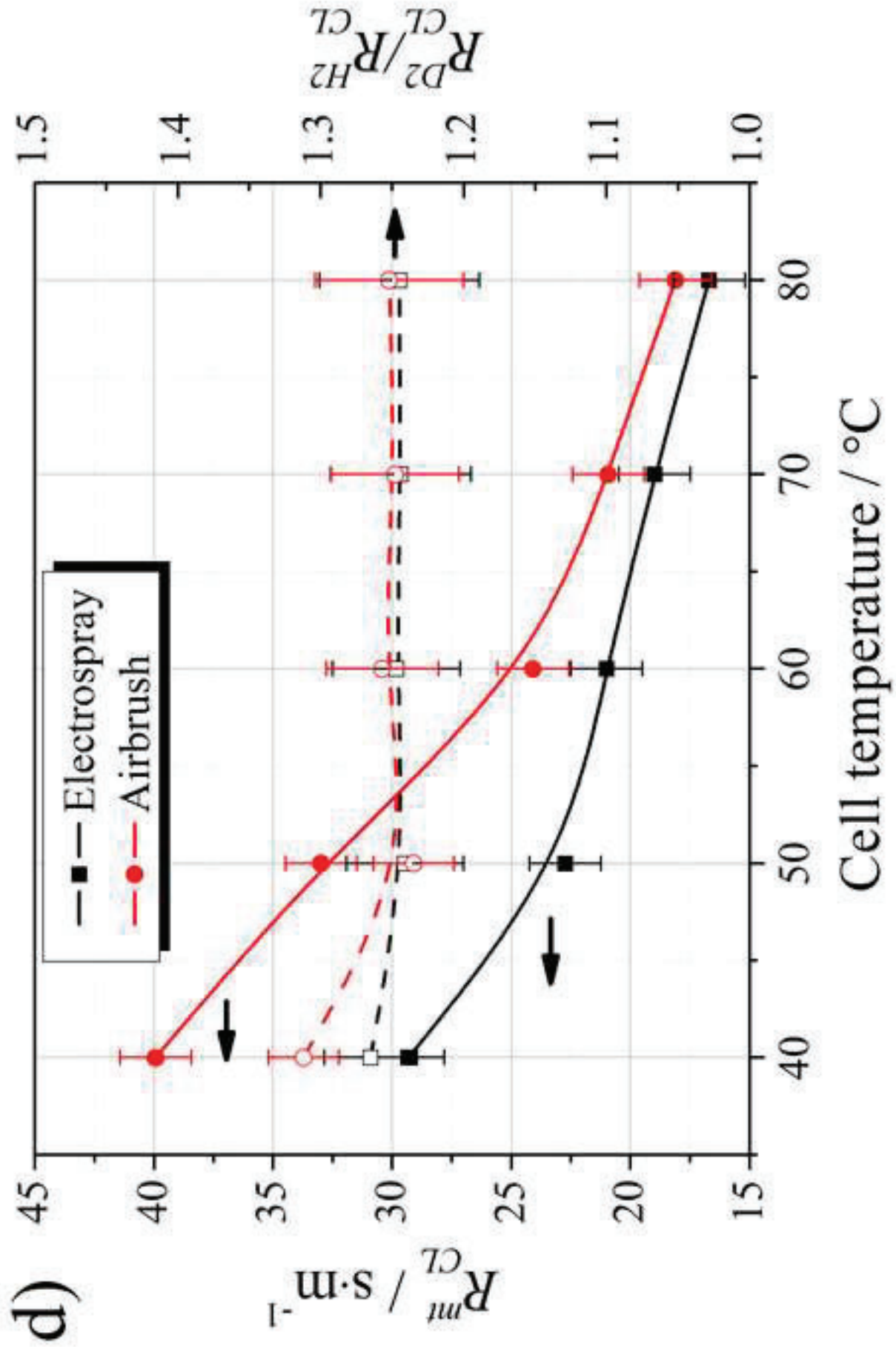
- 1
2
3
4
5
6
7
8
9
10
11
12
13
14
15
16
17
18
19
20
21
22
23
24
25
26
27
28
29
30
31
32
33
34
35
36
37
38
39
40
41
42
43
44
45
46
47
48
49
50
51
52
53
54
55
56
57
58
59
60
61
62
63
64
65
-
- [16] P. Ferreira-Aparicio, A.M. Chaparro, M. A. Folgado, J.J. Conde, E. Brightman, G. Hinds, Degradation Study by Start-Up/Shut-Down Cycling of Superhydrophobic Electro sprayed Catalyst Layers Using a Localized Reference Electrode Technique, *ACS Appl. Mater. Interf.* 9 (2017) 10626–10636.
- [17] M.A. Folgado, J.J. Conde, P. Ferreira-Aparicio, A.M. Chaparro, Single Cell Study of Water Transport in PEMFCs with Electro sprayed Catalyst Layers, *Fuel Cells* 18 (2018) 602-612.
<https://doi.org/10.1002/face.201700217>
- [18] T.A. Greszler, D. Caulk, P. Sinha, The Impact of Platinum Loading on Oxygen Transport Resistance, *J. Electrochem. Soc.* 159 (2012) F831-F840.
- [19] G.S. Hwang, A.Z. Weber, Effective-Diffusivity Measurement of Partially-Saturated Fuel-Cell Gas-Diffusion Layers, *J. Electrochem. Soc.* 159 (2012) F683-F692.
- [20] A.Z. Weber, A. Kusoglu, Unexplained transport resistances for low-loaded fuel-cell catalyst layers. *J Mater. Chem. A.* 2 (2014) 17207-17211.
- [21] A. Kongkanand, M.F. Mathias, The Priority and Challenge of High-Power Performance of Low-Platinum Proton-Exchange Membrane Fuel Cells, *J. Phys. Chem. Letters* 7 (2016) 1127-1137.
- [22] F.B. Spingler, A. Phillips, T. Schuler, M.C. Tucker, A.Z. Weber, Investigating Fuel-Cell Transport Limitations using Hydrogen Limiting Current, *Int. J. Hydrogen Ener.* 42 (2017) 13960-13969.
- [23] N. Nonoyama, S. Okazaki, A.Z. Weber, Y. Ikogi, T. Yoshida, Analysis of Oxygen-Transport Diffusion Resistance in Proton-Exchange-Membrane Fuel Cells, *J. Electrochem. Soc.* 158 (2011) B416-B423.
<https://doi.org/10.1149/1.3546038>
- [24] J.P. Owejan, J.E. Owejan, W. Gu, Impact of platinum loading and catalyst layer structure on PEMFC performance, *J. Electrochem. Soc.* 160 (2013) F824-F833.
- [25] D.R. Baker, D.A. Caulk, K.C. Neyerlin, M.W. Murphy, Measurement of Oxygen Transport Resistance in PEM Fuel Cells by Limiting Current Methods, *J. Electrochem. Soc.* 156 (2009) B991-B1003.
- [26] Y. Ono, T. Mashio, S. Takaichi, A. Ohma, H. Kanesaka, K. Shinohara, The analysis of performance loss with low platinum loaded cathode catalyst layer, *ECS Transaction* 28 (27) (2010) 69-78.
- [27] A.T.S. Freiberg, M.C. Tucker, A.Z. Weber, Polarization Loss Correction Derived from Hydrogen Local-Resistance Measurement in Low Pt-Loaded Polymer-Electrolyte Fuel Cells, *Electrochem. Comm.* 79 (2017) 14-17.
- [28] T. Schuler, A. Chowdhury, A.T. Freiberg, B. Sneed, F.B. Spingler, M.C. Tucker, K.L. More, C.J. Radke, A.Z. Weber, Fuel-cell Catalyst-Layer resistance Via Hydrogen Limiting-Current Measurements, *J. Electrochem. Soc.* 166(7) (2019) F3020-F3031.
- [29] A. Chowdhury, C. J. Radke, A. Z. Weber, Transport Resistances in Fuel-Cell Catalyst Layers, *ECS Transaction* 80 (8) (2017) 321-333. <https://doi.org/10.1149/08008.0321ecst>
- [30] R. Koestner, D.Cullen, R. Kukreja, S. Minko, H.M. Meyer, Z.Liu and K.L. More , High-Resolution Mapping of the PFSA Polymer Distribution in PEFC Electrode Layers, *ECS Trans.* 64 (3) (2014) 819-827.
- [31] D. A. Cullen, R. Koestner, R. S. Kukrej, Z. Y. Liu, S. Minko, O. Trotsenko, A. Tokarev, L. Guetaz, H. M. Meyer III, C. M. Parish, and K. L. Moref, Imaging and Microanalysis of Thin Ionomer Layers by Scanning

- 1
2
3
4
5
6
7
8
9
10
11
12
13
14
15
16
17
18
19
20
21
22
23
24
25
26
27
28
29
30
31
32
33
34
35
36
37
38
39
40
41
42
43
44
45
46
47
48
49
50
51
52
53
54
55
56
57
58
59
60
61
62
63
64
65
-
- Transmission Electron Microscopy, *J. Electrochem. Soc.* 161 (10) (2014) F1111-F1117.
- [32] A. Kusoglu, A. Kwong, K.T. Clark, H.P. Gunterman, A.Z. Weber, Water Uptake of Fuel-Cell Catalyst Layers, *J. Electrochem. Soc.* 159 (9) (2012) F530-F535.
- [33] J.J. Conde, A.M. Chaparro, P. Ferreira-Aparicio, Understanding the Behavior of Electro sprayed Carbon Black-Nafion Composite Layers, *Fuel Cells* 18 (2018) 627-639.
<https://doi.org/10.1002/fuce.201700218>.
- [34] J.J. Conde, P. Ferreira-Aparicio, A.M. Chaparro, Anti-corrosion coating for metal surfaces based on superhydrophobic electro sprayed carbon layers, *App. Mat. Today* 13 (2018) 100–106.
- [35] Y.-C. Park, H. Tokiwa, K. Kakinuma, M. Watanabe, M. Uchida, Effects of carbon supports on Pt distribution, ionomer coverage and cathode performance for polymer electrolyte fuel cells, *J. Power Sources* 315 (2016) 179-191.
- [36] A.M. Chaparro, B. Gallardo, M.A. Folgado, A.J. Martín, L. Daza, PEMFC electrode preparation by electro spray: Optimization of catalyst load and ionomer content, *Catalysis Today* 143 (2009) 237–241.
- [37] K. C. Neyerlin, W. Gu, J. Jorne, H. A. Gasteiger, Determination of Catalyst Unique Parameters for the Oxygen Reduction Reaction in a PEMFC, *J. Electrochem. Soc.* 153 (2006) A1955-A1963.
<https://doi.org/10.1149/1.2266294>.
- [38] M. Lee, M. Uchida, D.A. Tryk, H. Uchida, M. Watanabe, The effectiveness of platinum/carbon electrocatalysts: Dependence on catalyst layer thickness and Pt alloy catalytic effects, *Electrochim. Acta*, 56 (2011) 4783-4790.
- [39] T. Suzuki, S. Tsushima, S. Hirai, Fabrication and performance evaluation of structurally-controlled PEMFC catalyst layers by blending platinum-supported and stand-alone carbon black, *J. Power Sources* 233 (2013) 269-276.
- [40] F.A. Uribe, T.E. Springer, S. Gottesfeld, A microelectrode study of oxygen reduction at the platinum/recast-Nafion film interface, *J. Electrochem. Soc.* 139 (1992) 765-773.
- [41] E. Springer, A. Zawodzinski, M. S. Wilson, S. Gottesfeld, Characterization of Polymer Electrolyte Fuel Cells Using AC Impedance Spectroscopy, *J. Electrochem. Soc.* 143(2) (1996) 587-599.
- [42] A. Lasia, Impedance of porous electrodes, *J. Electroanal. Chem.* 397 (1995) 27-33.
- [43] W.G. Pell, A. Zolfaghari, B. E. Conway, Capacitance of the double-layer at polycrystalline Pt electrodes bearing a surface-oxide film, *J. Electroanal. Chem.* 532 (2002) 13-23.
- [44] F. Beck, M. Dolata, E. Grivei, N. Probst, Electrochemical supercapacitors based on industrial carbon blacks in aqueous H₂SO₄, *J. Appl. Electrochem.* 31 (2001) 845-853.
- [45] D. Quéré, Wetting and Roughness, *Annu. Rev. Mater. Res.* 38 (2008) 71–99.
- [46] M. Prat, T. Agaësse, Thin Porous Media, in: Kambiz Vafai (Ed.), *Handbook of Porous Media*, 3rd Edition, CRC Press, Boca Raton, 2015, pp. 89-112.



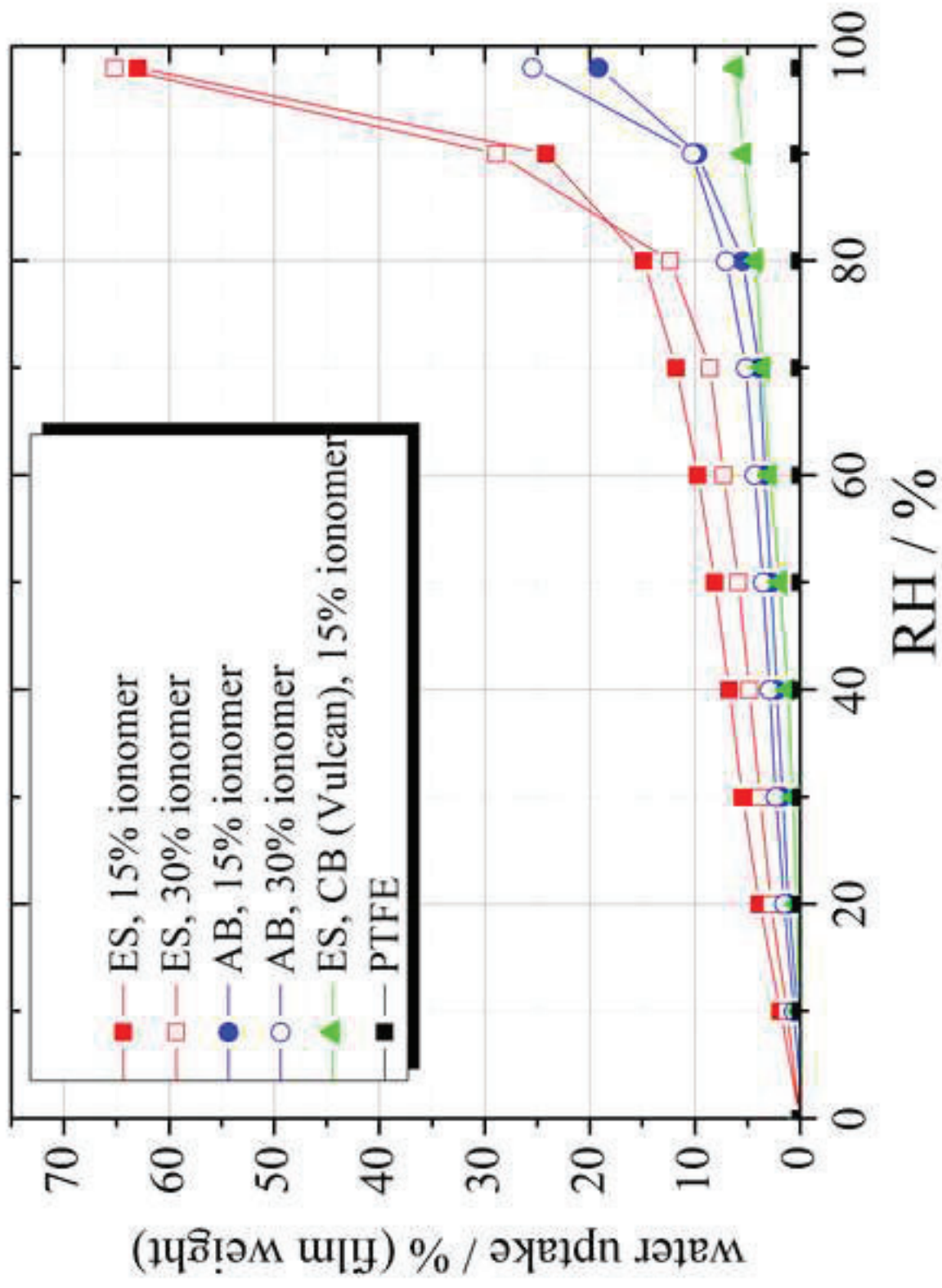




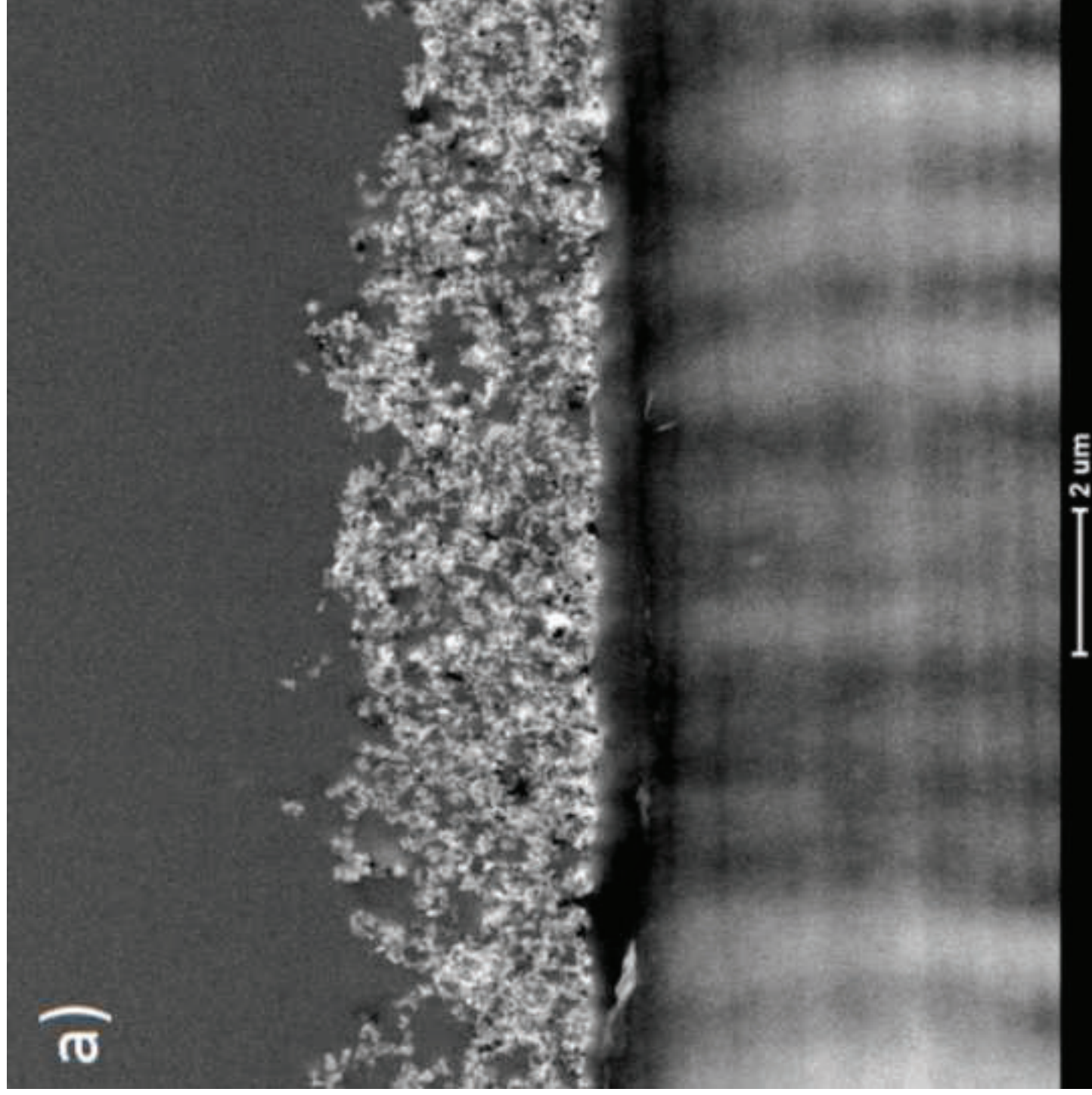


Figure(s) - provided separately
[Click here to download high resolution image](#)

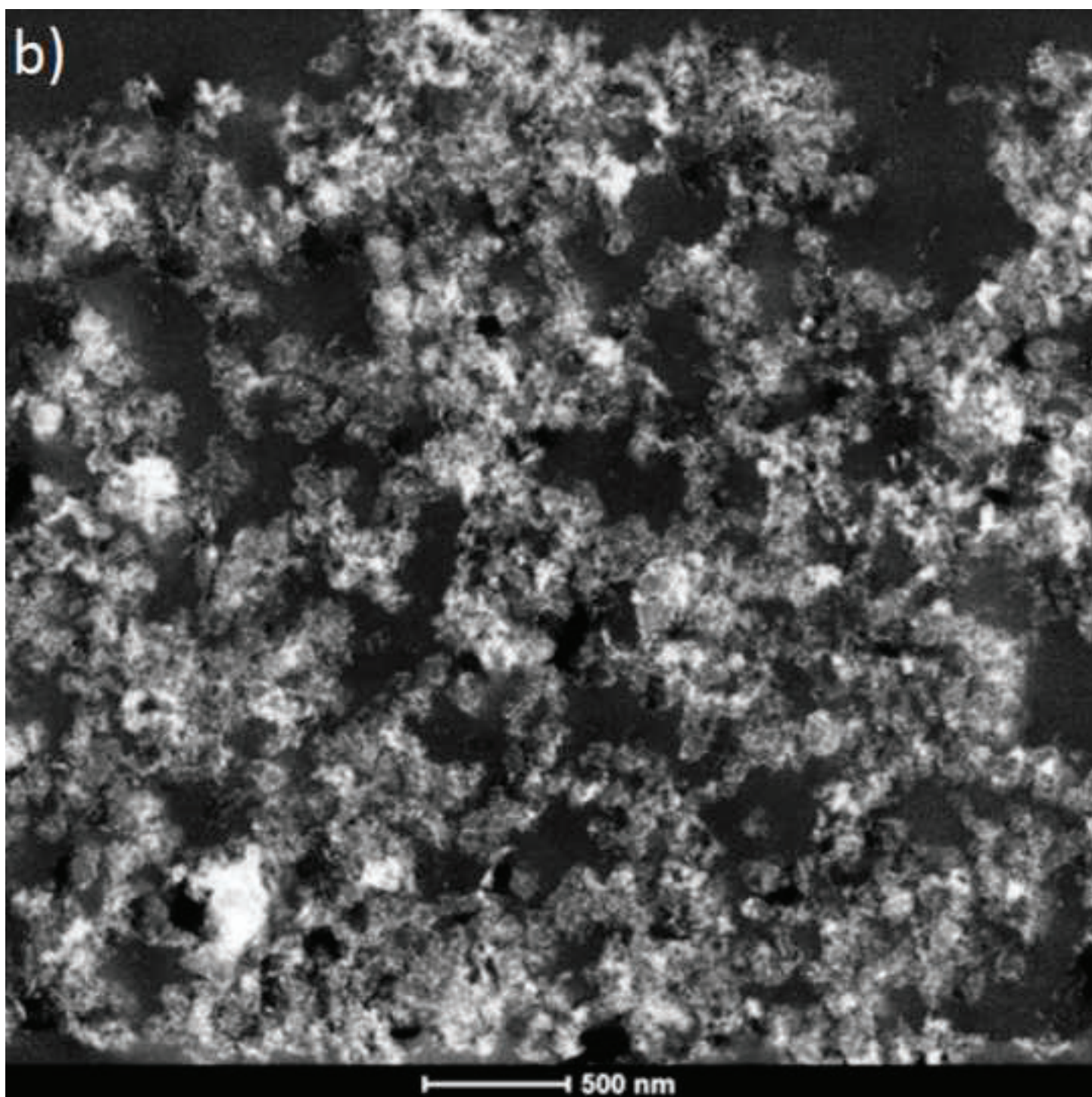
Figure(s) - provided separately
Click here to download high resolution image

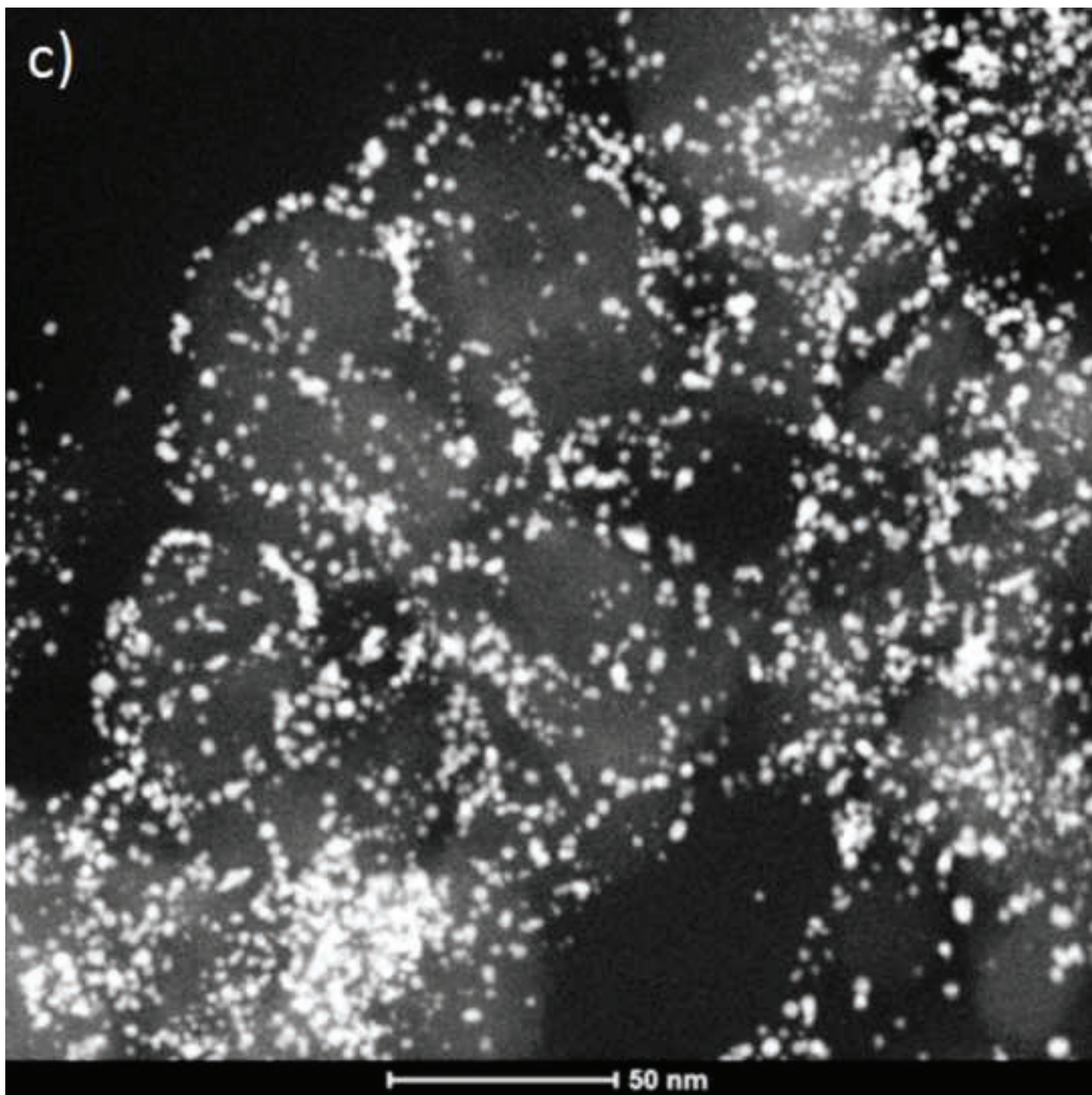


Figure(s) - provided separately
[Click here to download high resolution image](#)

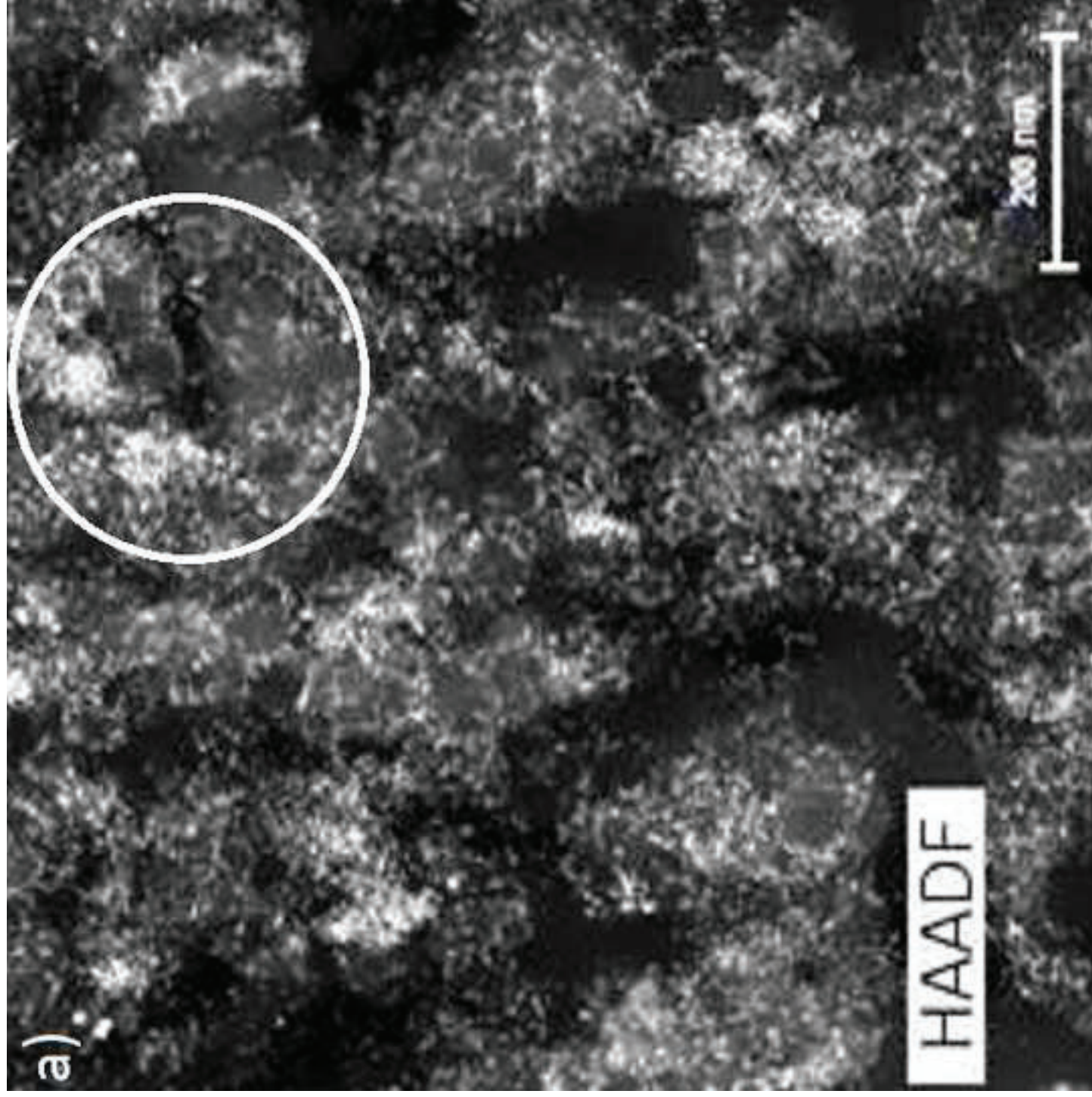


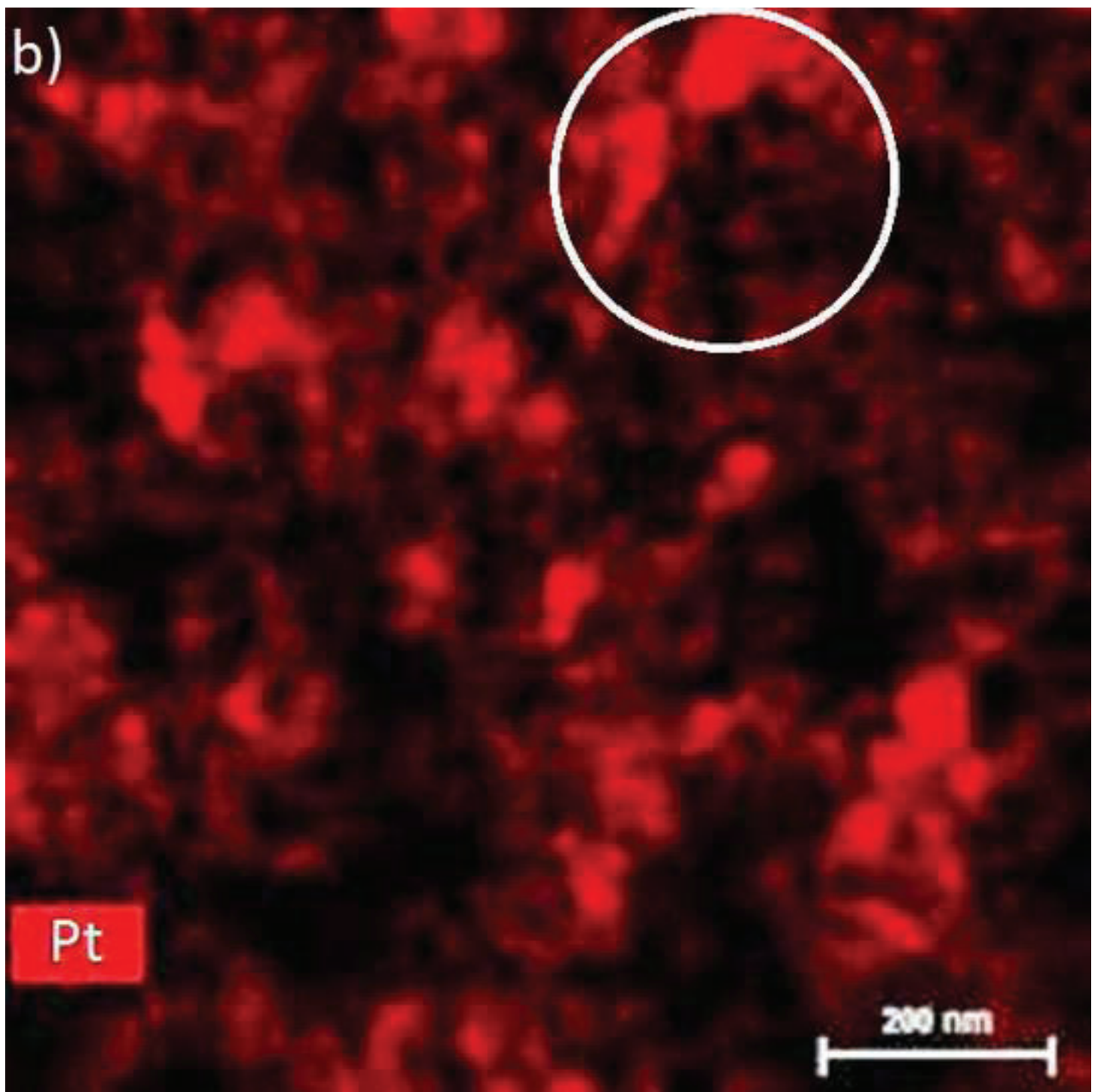
Figure(s) - provided separately
[Click here to download high resolution image](#)

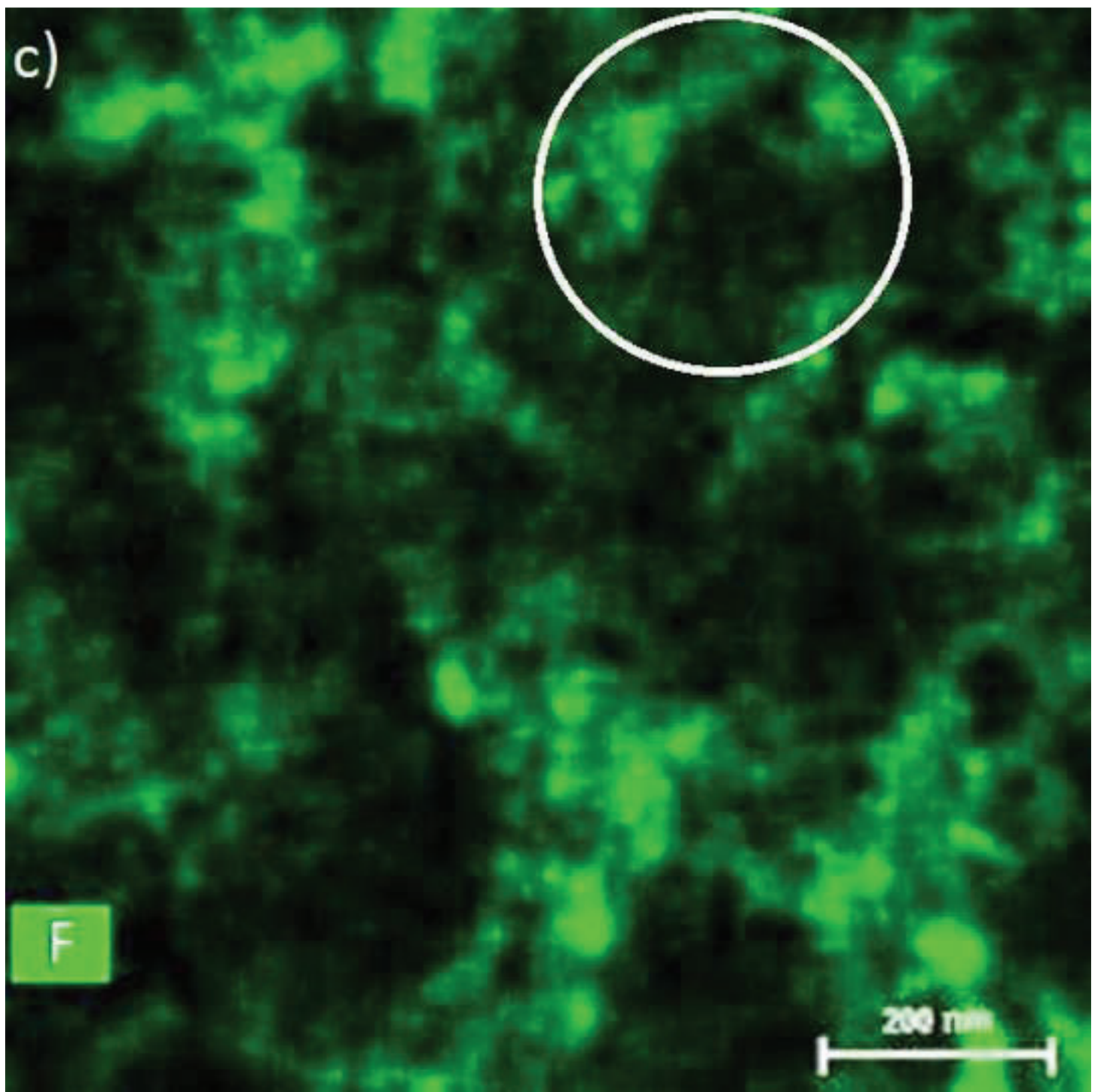


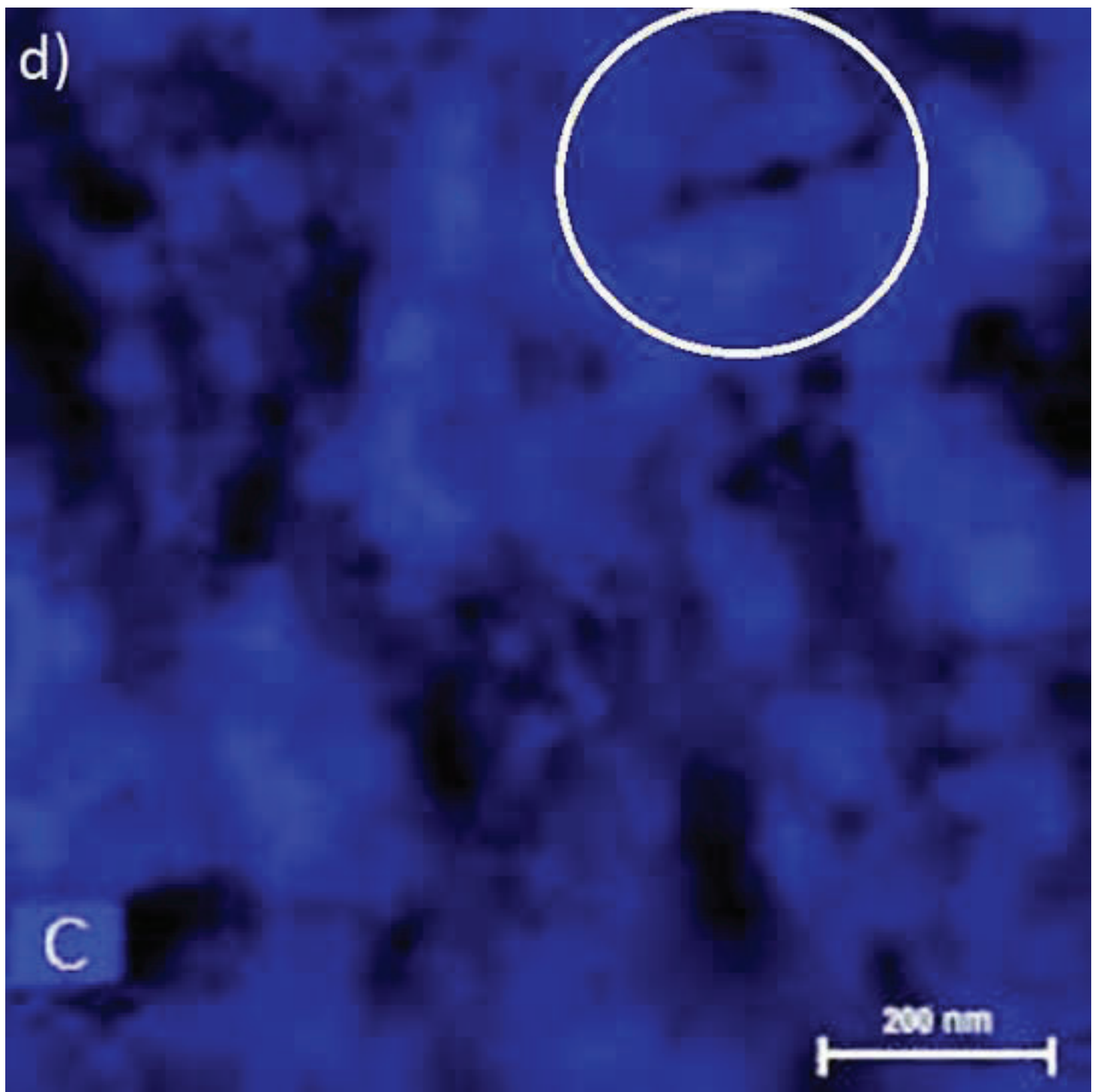


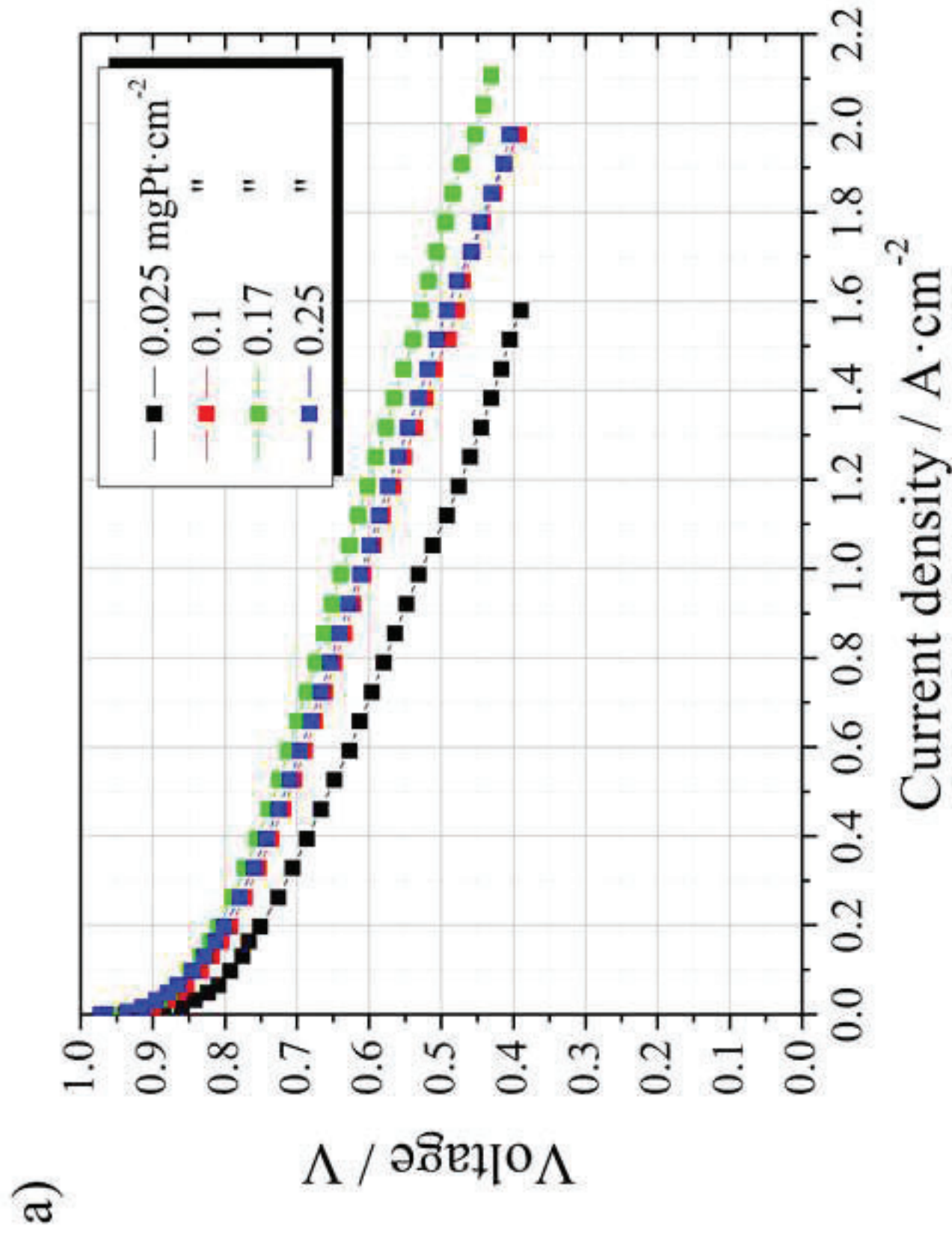
Figure(s) - provided separately
[Click here to download high resolution image](#)

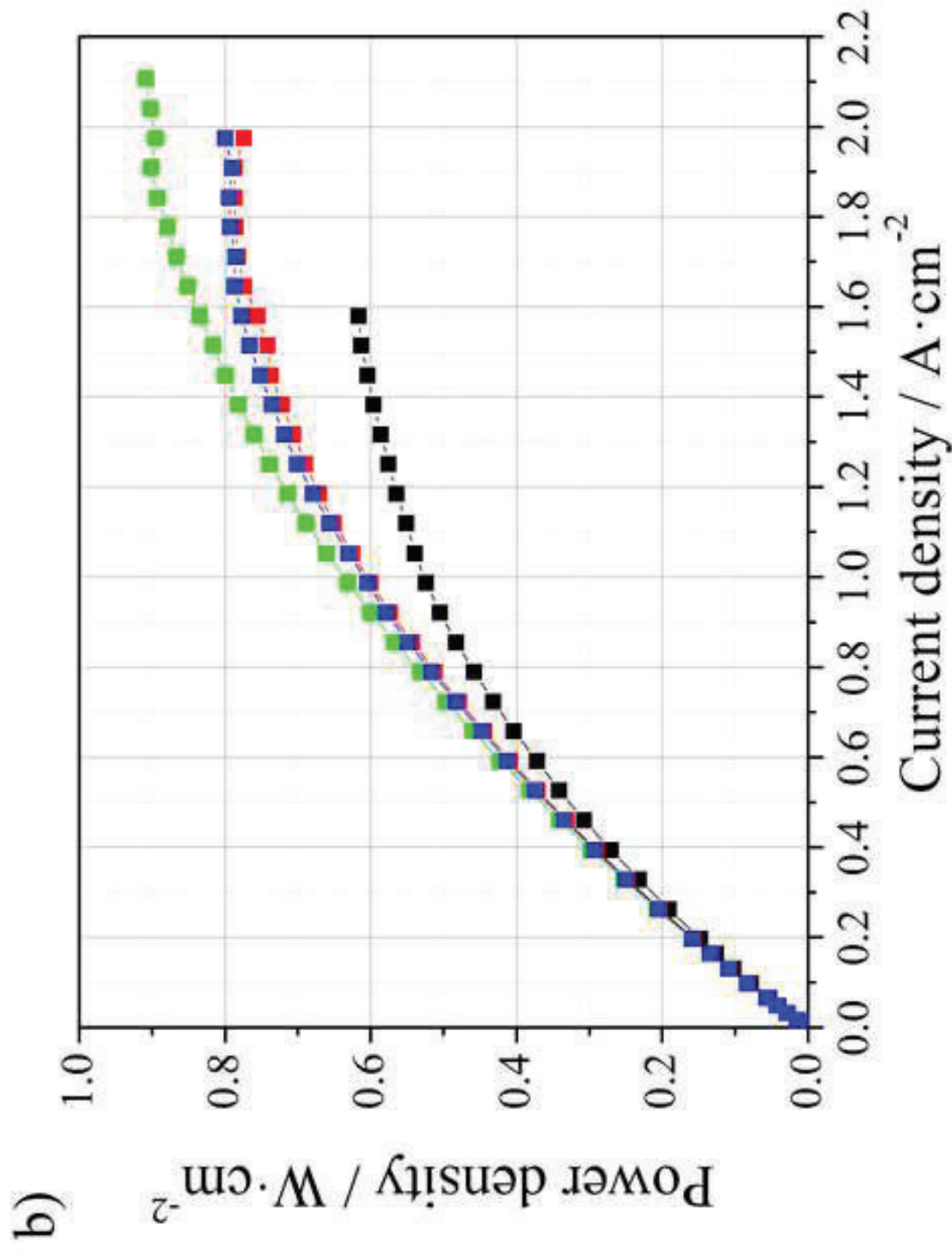


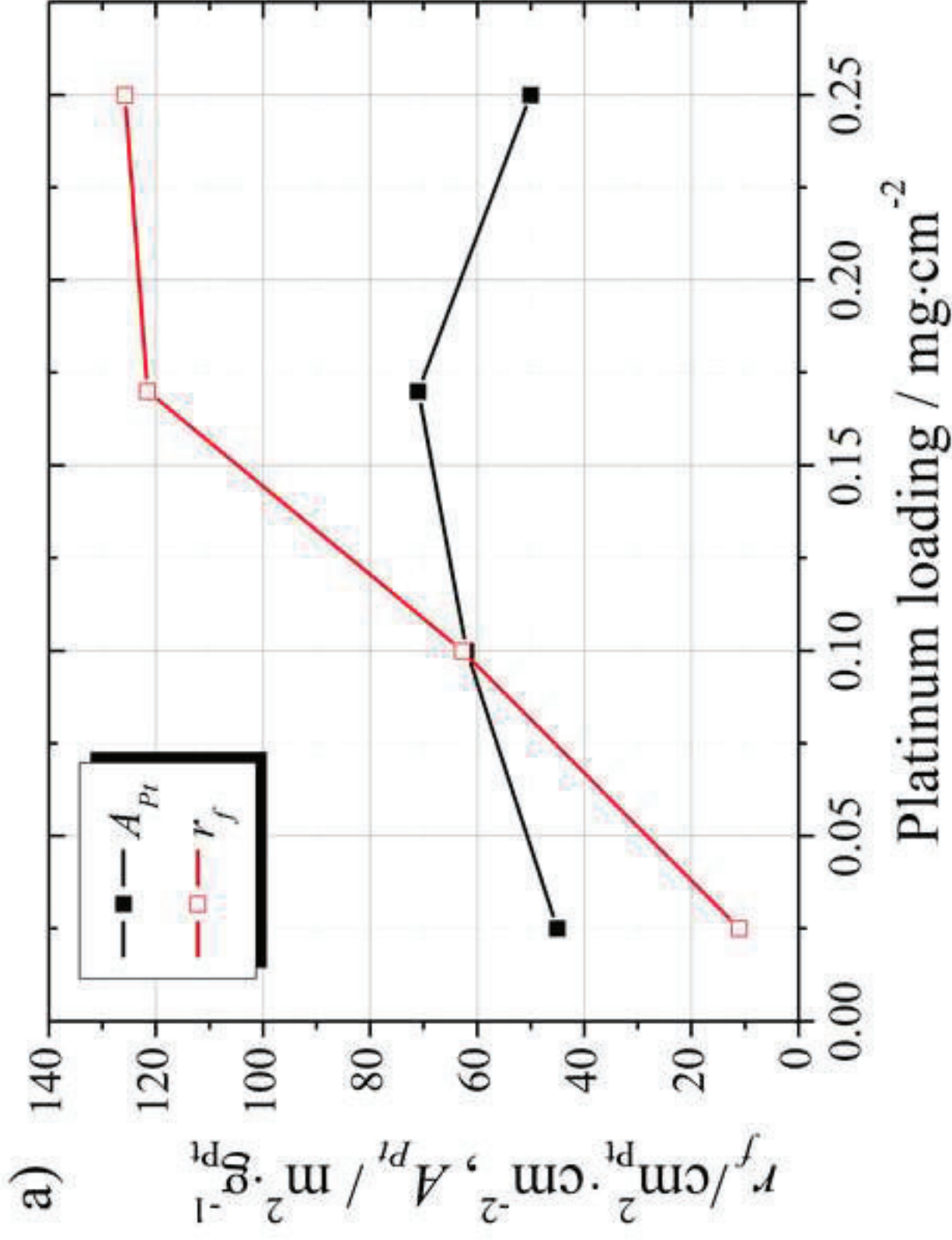


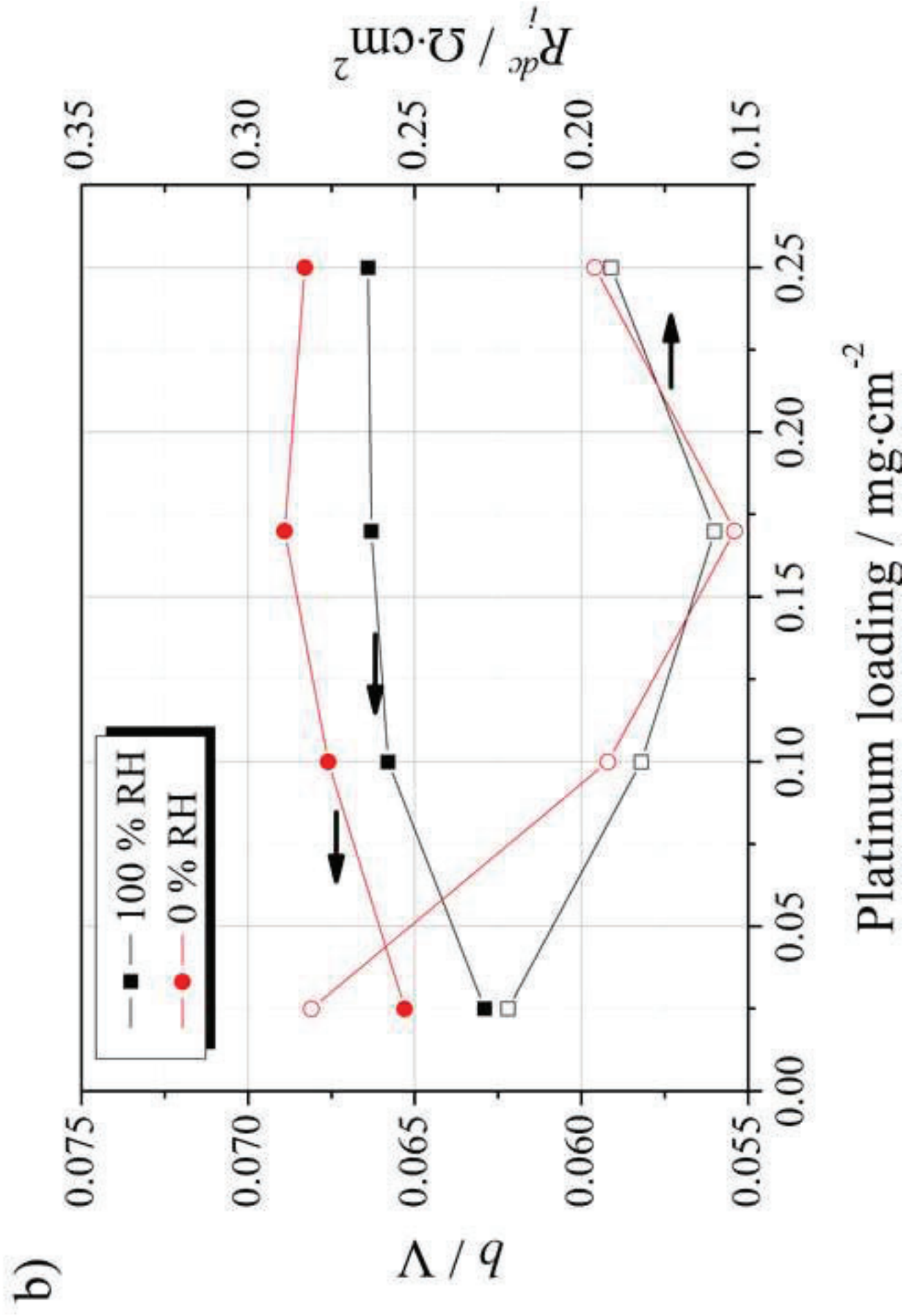


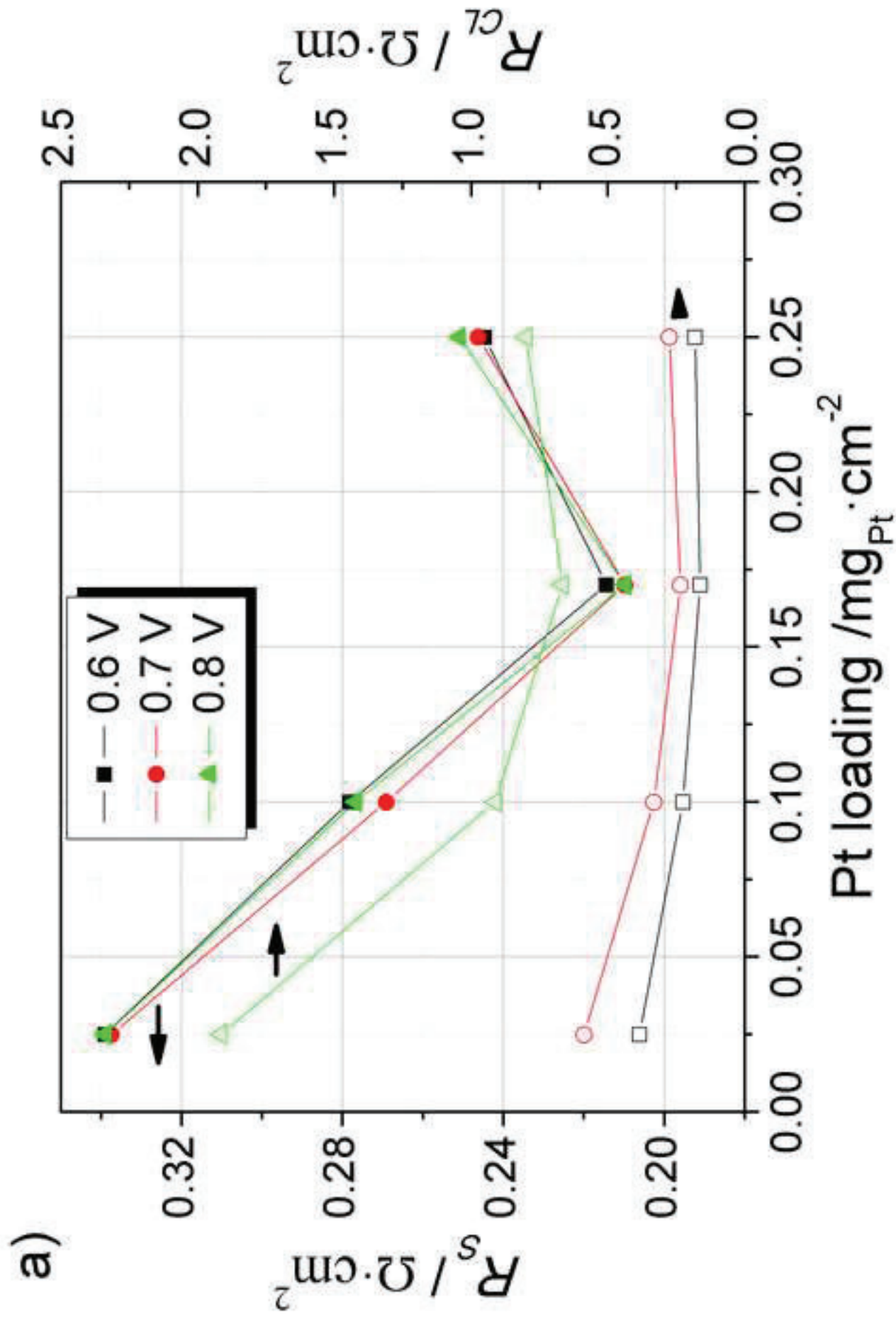


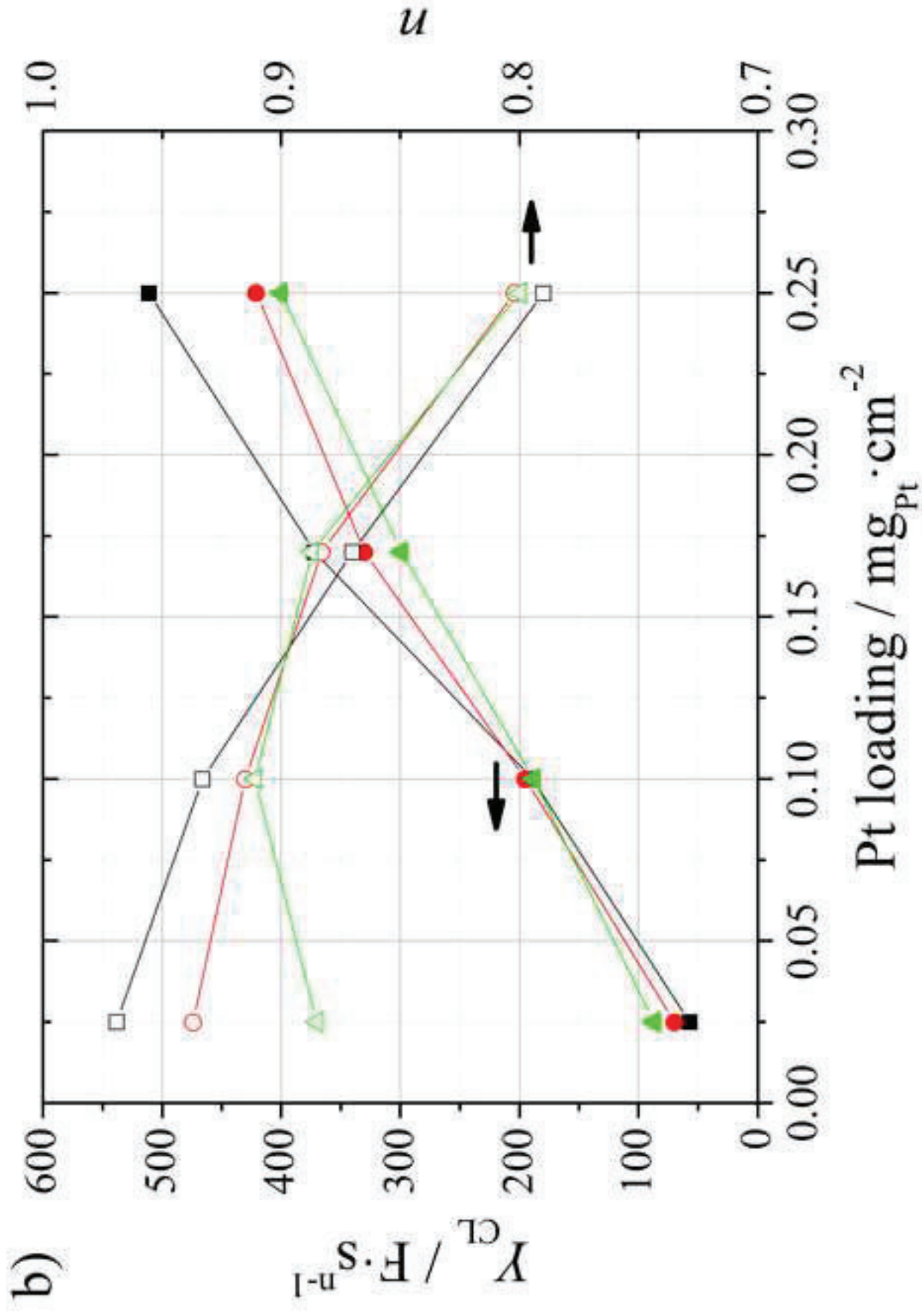


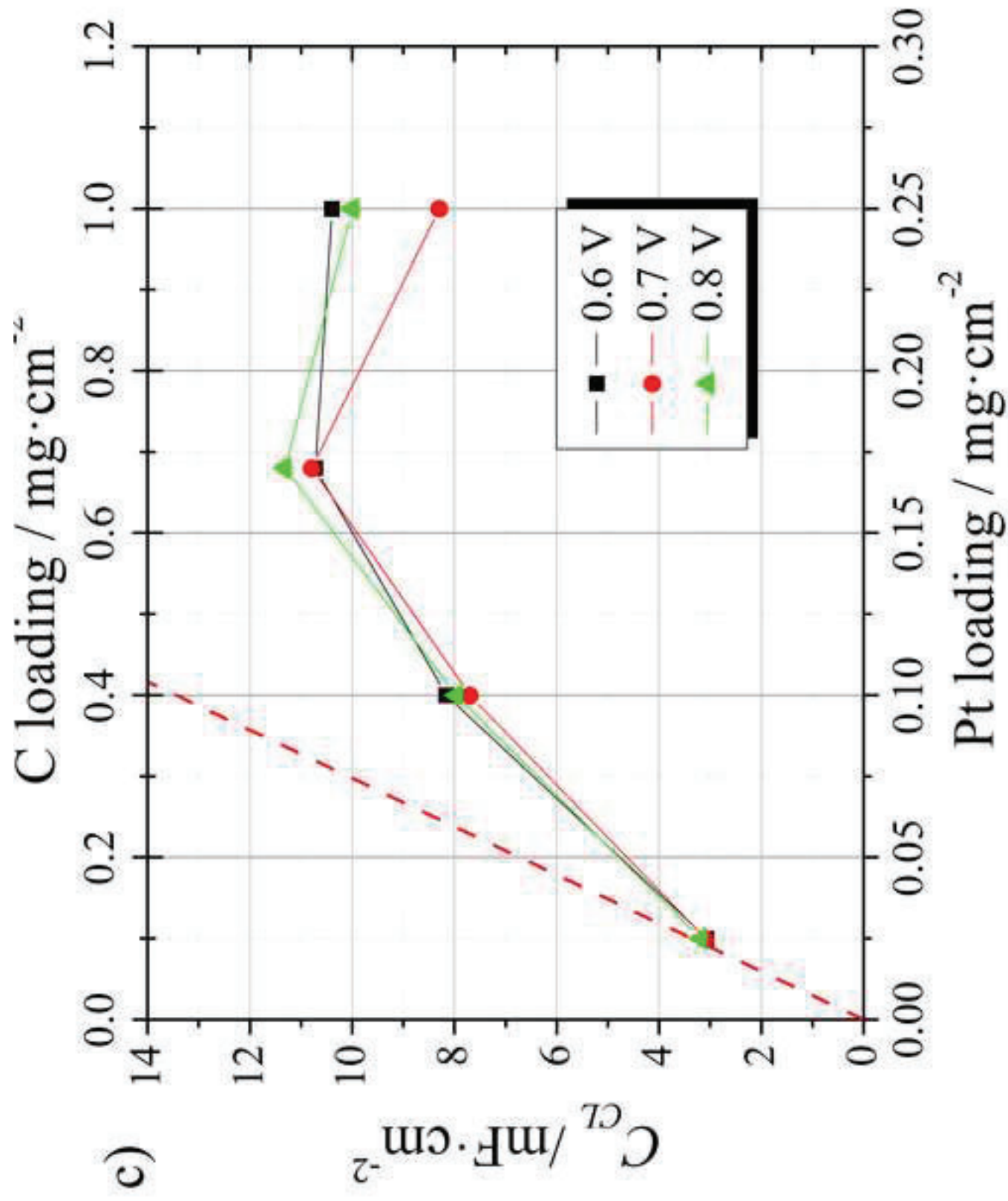












Figures captions

Fig.1. Mass-transport resistance (R_{cl}^{mt}), and molecular-weight specific resistances ratio ($R_{cl}^{D^2}/R_{cl}^{H^2}$, dashed line), as a function of ionomer concentration (a), Pt loading (constant Pt/C) (b), gas relative humidity (c), and cell temperature (d), for electro sprayed (black) and airbrushed (red) catalyst layers. In a) and b), measuring conditions are 80°C and 80% RH. In b), **electrosprayed films contain 15 wt% ionomer loading**, whereas the data of airbrushed film are taken from **ref.28, and correspond to films prepared with 37 wt% ionomer loading**. In c) and d), the catalyst layers have 0.25 mg·cm⁻² Pt loading, and 15 wt% ionomer concentration. The inset in (b) shows the R_{cl}^{mt} vs. $1/r_f$ plot (see the text).

Fig. 2. Water-vapor uptake desorption curves (see Supplementary Material, Fig. S2, for absorption curves **and results of λ calculation**), as a function of relative humidity, for catalyst layers deposited by electro spray and airbrushing. Results for the PTFE substrate are also included.

Fig.3. STEM images in cross section of an electro sprayed Pt/C + ionomer layer (0.025 mg·cm⁻², 15 wt% ionomer), at three different magnifications.

Fig.4. High-angle annular dark-field STEM image (a), and images of the distribution of Pt (b), F (c), and C (d). Circle for visual guide.

Fig.5. a) Polarization curves of single PEMFCs with electro sprayed catalyst layers of variable Pt loading in the cathode. b) Power density curves. Cells were tested at 80 °C, 1 bar_g, and 100% RH conditions, using H₂/O₂ (1.5/3.0 stoichiometry) in anode/cathode. Polarization curves at 0% RH are shown in Supplementary Material, Fig.S5.

Fig. 6.- a) Roughness factor (r_f) and mass specific electrochemical area (A_{pt}) of the electro sprayed catalyst layers of Fig.5 as a function of Pt loading. b) Tafel slope (b) and dc internal resistance (R_i^{dc}) at 100% RH and 0% RH, obtained from the least square fitting of polarization curves in Fig.5 to Eq.8.

Fig.7. a) Series resistance (R_s , full symbols) and catalyst layer resistance (R_{cl} , open symbols) as a function of Pt loading in the electro sprayed catalyst layer, at three cell voltages. b) Constant phase element parameters, Y_{cl} (full symbols) and n (open symbols), as a function of catalyst loading, at three cell voltages. Inset in a) shows the electric circuit used for the impedance analysis. Cell conditions as in Fig. 5.

Fig.8. Result of the application of Eq.9 to impedance analysis in Fig. 7b. Dashed red line indicates the estimated nominal capacitance of the carbon black phase.

Supplementary Materials

[Click here to download Supplementary Materials: Supplementary.docx](#)

Mass-transport properties of electrosprayed Pt/C catalyst layers for polymer-electrolyte fuel cells.

Julio J. Conde¹, M. Antonia Folgado¹, P. Ferreira-Aparicio¹, Antonio M. Chaparro^{1,*},

Anamika Chowdhury², Ahmet Kusoglu², David Cullen³, Adam Z. Weber²

1) Energy Department, CIEMAT, Avda. Complutense 40. 28040 Madrid, Spain

2) Energy Conversion Group, Energy Technologies Area, Lawrence Berkeley National Laboratory, 1 Cyclotron Road, Berkeley, California 94720, USA

3) Center for Nanophase Materials Sciences, Oak Ridge National Laboratory, Oak Ridge, Tennessee 37831, USA

Author contributions

Julio J. Conde: Investigation (all measurements type except STEM), data curation, conceptualization, formal analysis, methodology

M. Antonia Folgado: Investigation (single cell measurements), data curation, conceptualization

P. Ferreira-Aparicio: investigation (single cell measurements, thickness), supervision, funding acquisition, project administration

Antonio M. Chaparro: methodology, investigation (single cell measurements, thickness), supervision, validation, conceptualization, funding acquisition, project administration, original draft, review and editing

Anamika Chowdhury: Investigation (hydrogen limiting current measurements), data curation, conceptualization, formal analysis

Ahmet Kusoglu: Investigation (water uptake measurements), data curation, conceptualization

David Cullen: Investigation (STEM measurements), data curation, conceptualization

Adam Z. Weber: methodology (STEM, water-uptake and hydrogen limiting current measurements), conceptualization, supervision, validation, funding acquisition, project administration, review and editing